Nonlinear Processes in Geophysics (1997) 4: 137–155

Nonlinear Processes in Geophysics

© European Geophysical Society 1997

Factors affecting multiscaling analysis of rainfall time series

D. Harris, A. Seed*, M. Menabde, and G. Austin

Department of Physics, University of Auckland, Private Bag 92019, Auckland, New Zealand
*new affiliation: Hydrology Division, Bureau of Meteorology, GPO Box 1289 K, Melbourne, Victoria 3001, Australia

Received 22 May 1997 – Revised: 8 December 1997 – Accepted: 3 February 1998

Abstract. Simulations based on random multiplicative cascade models are used to investigate the uncertainty in estimates of parameters characterizing the multiscaling nature of rainfall time series. The principal parameters used and discussed are the spectral exponent, β, and the $K(q)$ function which characterizes the scaling of the moments. By simulating a large number of series, the sampling variability of parameter estimates in relation to the length of the time series is assessed and found to be in excess of 10%-20% for fields less than $\sim 10^4$ points in length. The issue of long time series which may consist of physically distinct processes with different statistics is addressed and it is shown that highly variable data mixed with an equal amount of less variable data of similar strength is dominated entirely by the statistics of the highly variable data. The effects on the estimates of β and $K(q)$ with the addition of white noise or the tipping bucket effect (quantization) can also be significant, particularly following gradient transformations. Some high resolution rainfall data are also analyzed to illustrate how a single instrumental glitch can strongly bias results and how mixing physically different processes together can lead to incorrect conclusions.

1 Introduction

Many geophysical fields appear geometrically complex involving high variability, intermittency, and the frequent occurrence of extreme values. Multiscaling analysis, on the other hand, presents a variety of techniques which can quantify these otherwise subjective properties. The multiscaling analysis of geophysical fields has become increasingly attractive to many researchers as a means of parameterizing the degree of intermittency, smoothness, and sometimes the extreme value statistics of highly variable fields (see Foufoula-Georgiou and Krajewski (1995) and Lovejoy and Schertzer (1995) for useful reviews). With the increasing use of these techniques it has become necessary to address the issues of robustness and the effects of noise on parameter estimates. In this paper random multiplicative cascade simulations are used to estimate how much uncertainty one can expect in the estimate of a parameter based on a single realization or sample of a field. A significant amount of uncertainty can be attributed to the fact that different realizations of a fixed process can lead to different parameter estimates as a consequence of their random nature.

Multiscaling analysis requires long data records to reduce the uncertainty in parameter estimates. On the other hand, rainfall processes are rarely stationary over long periods of time in the sense that rain associated with synoptic scale systems generally take less than one day to pass over a point. A careless combination of rainfall data into a single long time series may include a mixture of significantly different rainfall processes, each process with a potentially different multiscaling flavor. It is necessary, therefore, to assess the impact of mixing different rainfall processes on the estimated multiscaling parameters.

Rainfall estimates are also fraught with measurement errors and instrumentation artifacts. While working with imperfect instruments, it is important that the impact of these imperfections on the estimates of parameters used to describe the multiscaling behavior of the rainfields be clearly understood. This is particularly the case when comparing statistics of data from different instruments such as radar and rain gauges.

The overall objective of this paper is, therefore, to assess in the context of multiscaling time series:

1) the extent of the uncertainty of parameter estimates in relation to the length of data sequences,
2) the effect on parameter estimates of mixing physically distinct processes,
3) and the biases in parameter estimates due to noise and instrumental artifacts.

Correspondence to: G. L. Austin

Understanding these three technicalities is necessary in order to determine whether an observed difference in parameters from two data sets is likely to be significant or not.

1.1 Analysis Framework and Terminology

The analysis framework used here focuses on two properties of multiscaling fields. Firstly, a multiscaling field must have a Fourier power spectrum which is scaling or equivalently has the power-law form,

$$P(f) \sim f^{-\beta}, \tag{1}$$

over a certain range of scales. β estimated from rainfall time series have been observed to fall in a range between approximately 0.3 and 1.7 (Georgakakos et al., 1994; Lovejoy and Scherzter, 1995; Harris et al., 1996). Secondly, a field, R, is said to be multiscaling if its q^{th} order moments behave as,

$$\langle R(t)^q \rangle \sim (t/T)^{-K(q)}, \tag{2}$$

where t is the time resolution of the time series and T is the total time length (see Davis et al. (1994) for an instructive paper on multiscaling and the estimation of $K(q)$ which characterizes the multiscaling behavior of a field).

While the relation (2) is sufficient to determine a field as multiscaling, spectral analysis and, more specifically, the value of the spectral exponent, β, play an important role in the multiscaling characterization of rainfields. Theoretically it can be shown that fields which are multiscaling (i.e., obey (2) over a finite range) have $\beta < 1$ (e.g., Davis et al., 1994). Rainfields, on the other hand, often have $\beta > 1$ and in this case cannot be multiscaling (Menabde et al., 1997). Rainfields with $\beta > 1$ may have multiscaling generalized structure functions,

$$\langle |R(t+\tau)-R(t)|^q \rangle \sim \tau^{\zeta(q)} \tag{3}$$

where τ is the time lag between two measurements in a time series, $R(t)$. Fields having the property (3) over a finite range of lag, τ, are referred to as multiaffine (Benzi et al., 1993). In practice when a multiaffine field, R, with $\beta > 1$ undergoes a small scale absolute gradient transformation defined by

$$\Delta R_\tau(t) = |R(t+\tau)-R(t)|, \tag{4}$$

the resulting ΔR field will be multiscaling and have a scaling power spectrum with $\beta < 1$. In this case there exists a theoretical relation between $\zeta(q)$ for the multiaffine field and $K(q)$ for its gradients (Vainshtein, et al., 1994; Menabde et al., 1997),

$$K(q) + \zeta(q) = \zeta(1)q. \tag{5}$$

$K(q)$ is thus the main statistical characterization of multiscaling fields and is often used to characterize multiaffine fields as well. Sometimes one refers to the $K(q)$ function of a multiaffine field. In this case it is understood that the $K(q)$ characterizes the absolute gradient field, $\Delta R_\tau(t)$ of the multiaffine field, $R(t)$.

The terminology "broad sense" stationarity and nonstationarity to describe fields with $\beta < 1$ and $\beta > 1$, respectively has become popular recently (e.g., Davis et al., 1996b, p.108 and references therein) and can be used in place of the terms multiscaling and multiaffine used here. However this use of the words stationary and nonstationary is subject to an argument in semantics as it conflicts with previous and more accepted definitions of stationarity. For example, the Wiener-Khinchin theory of covariance and spectrum is applicable to stationary functions only (e.g., Mandelbrot, 1983, p. 351) and strictly speaking the usual Fourier power spectrum is not defined for nonstationary signals. Furthermore, the present authors refer to an interesting example of a stationary random process (Yaglom, 1987, p. 139) yet which has an asymptotically scaling power spectrum with $\beta > 1$ (Menabde et al., 1997). In essence, however, the authors mean the same thing by multiscaling and multiaffine here as the respective broad sense terms stationary and nonstationary used elsewhere (Davis et al., 1996b, 1994; Lavallée et al., 1993) and regard the nomenclature as still being in a state of flux.

An incentive for the multiscaling characterization of fields is that it allows one to build a cascade model which is able to reproduce the observed statistical characteristics of the field as embodied in the exponent, $K(q)$. $K(q)$ is a continuous function, thus in principle, requiring an infinite number of parameters. It is, however, possible to construct models characterized by a few parameters for which one can derive analytical forms for the $K(q)$ function involving the same modeling parameters. By fitting an analytical form to the observed data we can in principle retrieve one or more modeling parameters. The parameters analyzed in this paper are, therefore, the spectral exponent, β, $K(q)$, and the parameter(s) used to characterize $K(q)$.

At this time the most common model is based on discrete random multiplicative cascades. Other models include the continuous Universal Multifractals of Schertzer and Lovejoy (1987) and recent models which employ wavelet decomposition (Perica and Foufoula-Georgiou, 1996). In this paper only discrete multiplicative cascade models are used.

1.2 Overview

This paper is organized as follows: The next section discusses specific details concerning β and $K(q)$ estimation as well as the types of simulations used. Section 3 examines sampling variability in relation to time series length. Long time series are desirable from a statistical point of view yet analyzing time series long enough to encompass meteorologically different processes with different statistics may bias results. This issue of mixing

physically distinct processes with differing statistics is treated in Section 4. Noises and instrumental artifacts are discussed in Section 5. There are three effects considered in this section: The effect of quantization of data, additive white noise, and the effect of the previous two artifacts following the small scale absolute gradient transformation of a field. Illustrations of the effect of instrumental noise and artifacts are also provided using rain gauge and radar time series. Section 6 summarizes the important points made in the text and concludes the paper. An appendix contains a brief overview of some properties of canonical cascades pertinent to the analysis of such cascades in this paper.

2 Analysis Methods and Simulation

2.1 Spectral Analysis

A first step in the analysis of fields that may display multiscaling properties is to examine the behavior of the Fourier power spectrum. A scaling behavior of the power spectrum implies that there are no characteristic time scales, and, therefore, the time series may be statistically self-similar. In reality scaling is never perfect, and is usually restricted within a limited range which can be estimated from the power spectrum.

There are two methods used in this paper of reducing noise in the estimation of the power spectrum, and hence β. The first method employs the subdivision of the time series into smaller intervals. The spectrum of each interval is then averaged together to provide a power spectral density (PSD) with lower variance albeit with a smaller frequency range over which to observe scaling. This process, referred to here as subdivision, is common in spectral analysis and is done automatically using the SPCTRM.C program in Press et al. (1992), with no windowing.

The second method used in this paper to display a noise reduced spectrum over a larger frequency range is called octave binning (Davis et al., 1996). It is less common in spectral analysis because it reduces spectral resolution, an item of little concern for scaling, and is thus described here briefly for convenience (see Davis et al. (1996) for an extensive discussion).

For octave binning, the PSD is computed using SPCTRM.C (Press et al., 1992) with parameter $k = 1$, so that the time series is subdivided into two subsections. The PSD is then averaged into bins spaced logarithmically in frequency according to:

$$\bar{f}_m = \frac{1}{2^m} \sum_{j=2^m}^{2^{m+1}-1} f_j \ , \quad m = 1,2,\ldots,\log_2(N)-2. \tag{6}$$

and the power spectrum is averaged into bins according to

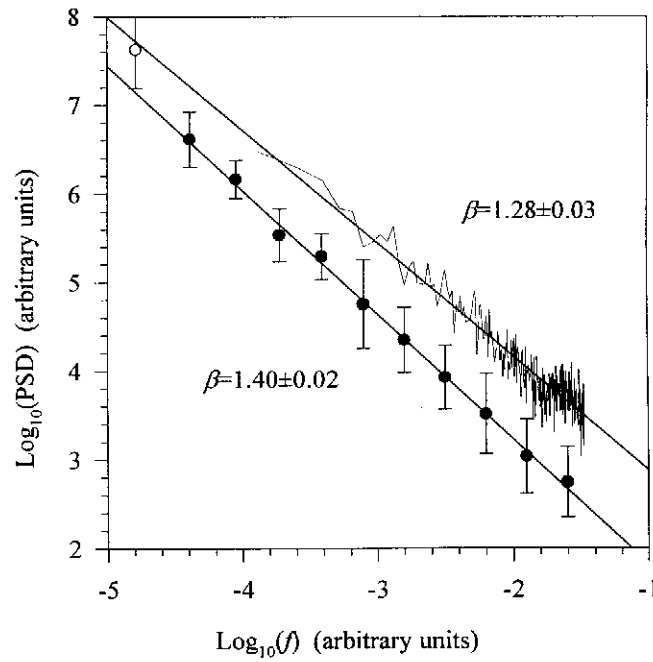

Fig. 1. Sample spectra computed from a 8192 point cascade simulation. The two plots represent the two methods of spectral noise reduction. The line spectrum is the result of subdividing the cascade into 16 pieces and averaging the spectrum of each piece. The octave binned spectrum is computed as described in the text. Only the filled points are included in the regression. The error bars are not used in the fitting procedure and are there for reference only. The cascade was constructed using the bounded log-normal model described in Section 2.3 with $\sigma = 0.8$ and $H = 0.3$.

$$\bar{P}_m = \frac{1}{2^m} \sum_{j=2^m}^{2^{m+1}-1} P(f_j) \tag{7}$$

and the variance in P_m for each bin is given by

$$\sigma^2_{P_m} = \begin{cases} P(f_1)^2, & m=0 \\ \dfrac{1}{2^m - 1} \displaystyle\sum_{j=2^m}^{2^{m+1}-1} P(f_j)^2 - \bar{P}_m^2, & m>0 \end{cases}. \tag{8}$$

Each bin involves the averaging of 2^m values, where m increases logarithmically with frequency for $m \gg 1$. An unweighted regression on the data from (6) and (7) is used to estimate β.

Fig. 1 shows an example of the two methods of spectrum estimation. Since Fig. 1 plots the logarithm of the power spectrum, the error bars shown in Fig. 1 are related to (8) by using the propagation of errors for logarithms (e.g., Taylor, 1982, Section 3.5),

$$\sigma_{\log_{10}\bar{P}_m} = \sigma_{P_m} / (\bar{P}_m \ln(10)) \ . \tag{9}$$

From an estimation point of view, a least squares regression estimate of β based on the subdivided spectra will be heavily biased towards the data at the high

frequency end of the spectra since this is where the bulk of the data are to be found. Fig. 1 shows such a bias in the spectra of a cascade where $\beta = 1.28$ for the subdivided spectrum and $\beta = 1.40$ for the octave binned spectrum. Octave binning has the effect of giving equal weight to all frequencies and would therefore provide estimates of β that are representative of the entire scaling range. The subdivided (non-binned) spectra are optimal for locating possible breaks in the scaling regime because of their high resolution.

2.2 Moment Scaling

Moment scaling analysis focuses upon $K(q)$ and its estimation which is usually followed by parameterizing $K(q)$ via least squares fitting of an analytical function, $K_a(q)$. Estimation simply involves finding the q^{th} moments of the field at the finest resolution and then degrading the field resolution by averaging nearest neighbors and re-computing the moments at this lower resolution. The $K(q)$ function is thus evaluated by plotting the q^{th} moment against the field resolution on a log-log plot and $K(q)$ is given by the slope of a linear regression through a scaling range. This presupposes the existence of a finite scaling range between two scales referred to here as t_{min} and t_{max}. It should be stressed that $K(q)$ is meaningless except over this finite scaling range and so this scaling range must be quoted for any $K(q)$ function or $K(q)$ parameterization. This is especially important as some geophysical fields (e.g., clouds (Davis et al., 1997) and possibly rainfall (Fabry, 1996)) may have more than one scaling range each with different $K(q)$. The scaling range which is conveniently quantified by the ratio, t_{max}/t_{min} (expressed in orders of magnitude), is more common as an indicator of the degree of scaling. Davis et al. (1996b) have established a criterion based on t_{max}/t_{min} with which to determine whether a field should be referred to as multiscaling or not. Other caveats regarding the reference to a field with having t_{max}/t_{min} as scaling exist in the literature (e.g., Hamburger *et al.*, 1996).

In principle, $K(q)$ is an unknown function defined for all $q \in (-\infty, +\infty)$ with $K(0) = K(1) = 0$ and thus requires an infinite number of parameters to describe. In practice, however, curve fitting methods can be used to parameterize $K(q)$ and analytical forms, $K_a(q)$, can be theoretically derived for specific cascade models such as the log-normal model below and other models (Gupta and Waymire, 1993; Schertzer and Lovejoy, 1987) which are often based on only one or two parameters. When fitting $K_a(q)$ to the observed $K(q)$, finite data length and the presence of noises and zeroes, place restrictions on the range of q over which $K_a(q)$ may be reasonably fit to the computed $K(q)$. In the case of the presence of zeroes, $K(q)$ cannot be computed at all for negative q and one will also have $K(0) < 0$, while the theoretical forms have $K_a(0) = 0$. This means that there will be some $q_{min} > 0$ and $K_a(q)$ cannot be realistically fit to $K(q)$ for $q < q_{min}$. Low level noise contributes greatly to the low order moments ($q << 1$) and will similarly introduce a q_{min} below which $K(q)$ may deviate strongly from any $K_a(q)$ or bias parameter estimates. In the absence of zeroes q_{min} can obviously be negative. In any case, $K(q)$ for $q < q_{min}$ reflects either measurement effects rather than the real field or the presence of zeroes, which may be real, yet for which cascades without an atom at zero cannot model. This is addressed further below. Since rain measurements very often contain zeroes, q is restricted here to non-negative values.

In addition to a lower limit on q, there is an upper limit on q above which $K(q)$ becomes increasingly linear. This is a result of the fact that taking the q^{th} power of a field for $q >> 1$ enhances the relative contribution to the q^{th} moment of the few, or even single, most extreme value(s) of the field. Clearly, fitting a curved function to the observed $K(q)$, as will be done below, requires limiting the maximum value of q, referred to here as q_{max}, up to which the fit is performed. The value of q_{max} is important for fitting the analytical $K_a(q)$ to the observed $K(q)$. For example, the analytical form, $K_a(q)$, for a log-normal cascade process is a parabola (see below) and fitting a parabola to a curve which is linear for $q >> q_{max}$ biases the parameter estimate characterizing the curvature of the parabola. In previous works, a maximum value of q was derived within the framework of singular measures (Schertzer and Lovejoy, 1992) and referred to as q_s and is dependent on the number of samples or realizations used to compute $K(q)$ and if the model parameters are known (i.e., in the case of a cascade field) a simple relation for q_s may be derived (e.g., see Lovejoy and Schertzer (1995) for the case of the log-stable model) and in general provides a good estimate. One of the matters addressed below, however, is that q_{max} is not only dependent on the amount of individual realizations but also strongly dependent on the specific data set (realization) from which $K(q)$ is estimated.

Since q_{max} depends on the presence of extreme values in the data set and since the ratio of the maximum to the mean may fluctuate between data sets with similar multiscaling properties (in the statistical sense), so too will q_{max} (see Section 3.2 below). There is thus an advantage to estimate q_{max} for a particular data set before fitting $K_a(q)$ with the added incentive that q_{max} is in itself and interesting property of the field. There is no universally accepted manner in which to estimate q_{max} but a few simple methods explored for this study are briefly described here, two of which are used and discussed further below in Section 3.2.

One method involves computing $K(q)$ up to a very large value of q and then begin by fitting $K_a(q)$ to $K(q)$ over a small range of q about the mean, $q = 1$, for example. The process continues by iteratively increasing the range by a small amount and repeating the fit each time until such time that $K_a(q)$ differs from $K(q)$ by a certain amount. This method can, in principle, also be used to estimate q_{min} as

well as q_{max}. Another simple method involves establishing a criterion based on the original data based on how much the data contributes to each moment. For example, q_{max} can be the moment for which the top 10% of the data contributes to 90% of the moment. Use of such a criterion also gave reasonable results. Other methods investigated but not used below reduce the problem to one of nonlinear regression. One may employ change-point fitting methods in which one fits $K_a(q)$ to $K(q)$ for $q \leq q_{max}$ and fits a straight line, $aq + b$, to $K(q)$ for $q > q_{max}$ with the requirement that $a = K'(q_{max})$. In this case, however, one should expect a regime near q_{max} with significant fit residuals where $K(q)$ is not exactly linear yet is not well described by $K_a(q)$. Along the same lines but more complex, one can fit a function, $y = K_a(q)f(q - q_{max}) + a(q - b)(1 - f(q - q_{max}))$ where $f(x)$ is a continuous function $f(x) \sim 1$ for $x << 0$, $f(x) \sim 0$ for $x >> 0$ and a, b are additional fit parameters. This also gave inconsistent results, occasionally giving noticeable residuals.

2.3 Cascade Simulations

There are many cascade models which can be used for this purpose, and some have greater success than others at reproducing the particular characteristics of rainfall. The point to be made here, however, is that the fields which are constructed below provide plausible time series of rainfall which could have occurred in reality in the sense that they reproduce the statistical features being studied. Simplicity was a factor in the choice of models so as not to be distracted from the task at hand which is to investigate the certainty of estimated parameters and their sensitivity to measurement effects.

The one dimensional random multiplicative cascades used here employ the usual construction method found elsewhere in the literature (e.g., Gupta and Waymire, 1993; Davis et al., 1994; Harris et al., 1996) in which an interval with mean, R_0, is subdivided into, say, two halves and each half is multiplied by random weights $W(1)$ and $W(2)$, respectively. Each half is then divided again into halves and multiplied again by weights. This procedure is repeated for as many steps as desired.

Two types of cascade are considered which enable to simulate either multiscaling or multiaffine fields. In the first case when the random weights, W, are independent and identically distributed (iid.) at each step in the cascade the resulting field will be statistically self-similar by construction and will be multiscaling. For the purposes of illustration in this paper a simple case is sufficient in which the random weights are log-normally distributed.

Multiaffine fields are harder to create and current methods of modeling them are not ideal. Two methods found in the literature are frequently used to generate such fields: Firstly the method of power-law filtering or H-filtering (Schertzer and Lovejoy, 1987; Lavallée et al., 1993; Davis et al., 1996b) and secondly the method of bounded cascades (Cahalan et al., 1989; Marshak et al., 1994 and references within). The first is analogous to a popular algorithm for generating fractional Brownian motion where a field is transformed in three steps by taking 1) the Fourier transform of a field, 2) multiplying each Fourier frequency component by f^H, $H > 0$, and then 3) taking the inverse Fourier transform.

The other method is more recent and more direct in that the cascade method itself is altered to produce fields with $\beta > 1$ directly without the need to work in Fourier space. In essence the generator is changed at each step thereby producing a progressively smoother signal as the cascade progresses to smaller scales. This has to be done in a fashion so as to retain the scaling of the power spectrum. This can be accomplished by decreasing the variance of W in a power law fashion with each successive step in the cascade. Conceptually, the bounded cascades reflect the observation that most rainfall (i.e., that with $\beta > 1$) variability decreases with scale and consequently has a steeper power spectrum than multiscaling fields.

In practice both methods produce fields whose absolute gradients are not perfectly multiscaling over the entire range of scales modeled but show a reasonable degree of scaling over a limited range of over two orders of magnitude for a field which spans nearly four orders of magnitude (see below). Both the power law filtering method and the bounded cascade methods described above were assessed and found to give similar limited scaling ranges.

For simplicity, the model used in all the cases studied here is a discrete cascade with a log-normal generator with the same parameters used by Gupta and Waymire (1993). The cascades for generating both multiscaling and multiaffine fields are canonical, (i.e., the expectation of the weights, $\langle W \rangle$, is equal to one but the average at each step may not be exactly equal to one (Mandelbrot, 1974)). For bounded cascade simulations, the log-normal generator can still be employed and this is explained below. While in this paper the simulation is restricted primarily to the two models described below, to ensure that results are not specific to the choice of generator, most of the analysis was repeated on models with different generators including log-stable (Schertzer and Lovejoy, 1987; Gupta and Waymire, 1993), log-gamma (Saito, 1992), and microcanonical models. Relevant results using these additional generators are mentioned where appropriate.

2.3.1 Log-normal Cascades for Creating Multiscaling Fields ($\beta < 1$)

Log-normal multiplicative cascades used in these studies are generated with multiplicative weights, W, at each step given by

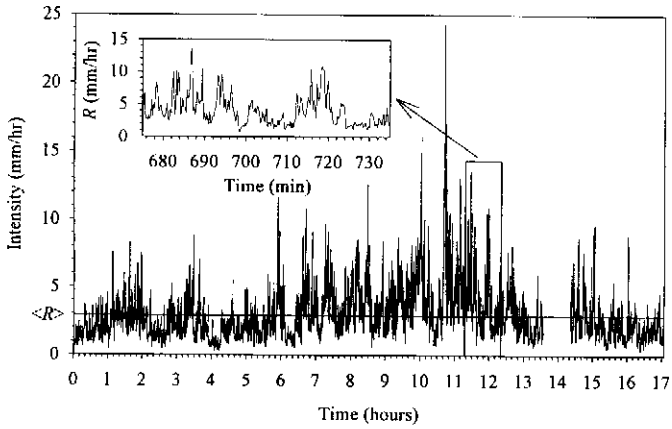

Fig. 2. A 4096 point log-normal cascade simulation of rainfall ($\sigma = 0.2$). The simulation has a $K(q)$ function and β similar to that computed for a stratiform rainfall event. For this particular cascade, β was estimated to be $\beta = 1.1 \pm 0.2$. The horizontal line represents the mean rain rate, $\langle R \rangle$ = 2.93 mm/hr. The fact that β can exceed unity for a canonical cascade is discussed in the Appendix.

$$W = e^{(\sigma X - \sigma^2/2)}, \tag{10}$$

where X is $N(0,1)$. The variance of the generator distribution is a function of σ, and in general small sigma leads to less intermittency since the resulting random weights are all closer to unity. This is a canonical cascade with $\langle W \rangle = 1$ ensured by the normalization factor of $\sigma^2/2$.

Fig. 2 shows some simulated rainfall using a log-normal cascade with $\sigma = 0.2$. The generator parameter, σ, was chosen to produce time series with a low degree of intermittency similar to the main divide rain gauge data in Harris et al. (1996, Figures 2 and 3) where $\beta < 1$.

The analytical function, $K_a(q)$, for the log-normal model is given by

$$K_a(q) = \log_b \langle W^q \rangle = \frac{\sigma^2}{2 \log b}(q^2 - q), \ \sigma > 0, \tag{11}$$

where W is the multiplicative weight in (10) and b is the branching number as described in Gupta and Waymire (1993) ($b = 2$ for all cascades herein). Equation (11) can be used to estimate the log-normal cascade parameter, σ. Strictly speaking this relationship assumes that the cascade has been constructed using an infinite number of steps (Gupta and Waymire, 1993; Kahane and Peyriere, 1976) and is also restricted to an upper limit on $q < q_{crit}$, $q_{crit} = K(q_{crit}) + 1$, where the divergence of moments occurs (Mandelbrot, 1974; Gupta and Waymire, 1993; Kahane and Peyriere, 1976). However, for practical purposes, cascades of 10 to 20 steps are more common, and thus the value of σ used to construct the cascade will not be retrieved exactly. There is a bias between the simulated σ and retrieved σ which decreases with increasing number of steps in the cascade. It is important to take this bias into account if one is trying to simulate a field with specific parameters. The reason for this bias is derived as a property of canonical cascades in the Appendix.

Since $\beta = 1 - \log_b \langle W^2 \rangle = 1 - K(2)$ (e.g., Davis et al., 1994),

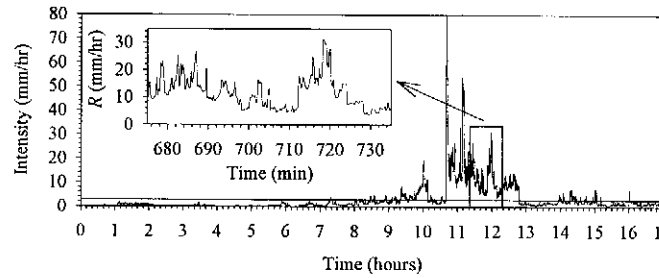

Fig. 3. Log-normal bounded cascade simulation of rainfall ($\sigma = 0.9$, $H = 0.3$). The simulation has a $K(q)$ function and β similar to that computed for a series of convective showers. For this particular cascade, β was estimated to be $\beta = 1.3 \pm 0.1$. The horizontal line represents the mean rain rate, $\langle R \rangle = 2.99$ mm/hr.

$$\beta = 1 - \frac{\sigma^2}{2 \log b}(2^2 - 2) = 1 - \frac{\sigma^2}{\log b}, \ \sigma > 0. \tag{12}$$

This result can be derived for the log-normal generator and other cascade generators using results in Gupta and Waymire (1993). The bias referred to in the Appendix is noticeably greater for β than for $K(2)$ (in the opposite direction) and so on the average $\beta + K(2)$ is greater than unity, although is sometimes less than unity.

For this particular model a simple relation exists for q_{max} using the theoretical relation derived for log-stable models (e.g., Lovejoy and Schertzer, 1995, equation (14a)) with $\alpha = 2$ (i.e., log-normal limit) and is referred to here as q_s to remain consistent with previous literature and to distinguish from empirically found q_{max}. For the log-normal model,

$$q_s = \frac{\sqrt{2 \log b}}{\sigma}. \tag{13}$$

2.3.2 Bounded Cascades for Creating Multiaffine Fields ($\beta > 1$)

In terms of reproducing the correct statistics and realistic looking rain gauge time series, good results are obtained using an alpha model (Schertzer and Lovejoy, 1987; Gupta and Waymire, 1993) modified to a bounded cascade as in Menabde et al. (1997). The model used in this study is slightly different in that the weights, W, vary as

$$W_k = 1 + (W_0 - 1) 2^{-(k-1)H}, \ k = 1,2,\ldots, \tag{14}$$

where W_0 can be any of the usual random weights used for self-similar multiplicative cascades and is normalized so that $\langle W_0 \rangle = 1$. H determines the slope of the power spectrum of the final multiaffine field. The higher the value of H, the greater the slope and hence the smoother the field will be. Again for simplicity and familiarity, W_0 is chosen to be log-normally distributed as in (10) above. Fig. 3 shows a typical time series generated using this method based on model parameters derived from a sequence of convective showers.

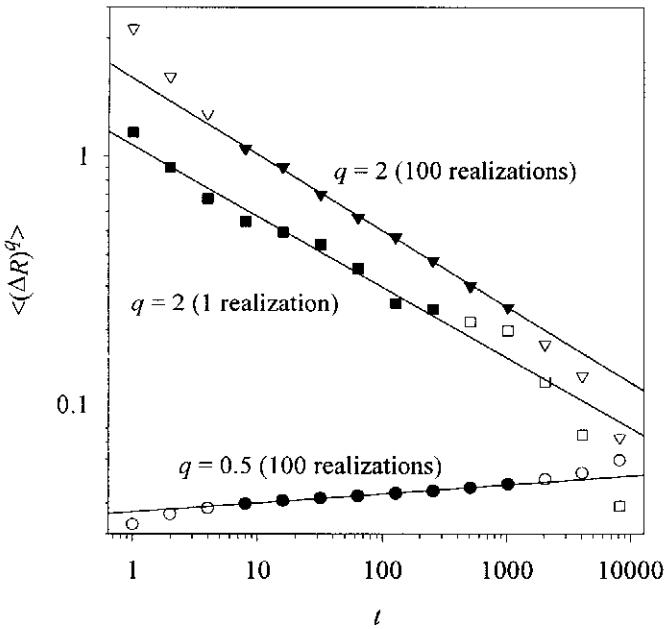

Fig. 4. Moment scaling for bounded cascades. The plots show the moment scaling for an ensemble of 100 realizations (circles and triangles) of 8192 point bounded cascades of the type used in the text with σ=1.4 and H=0.3. Also shown is the result for a single realization (squares) by generating an 18 step cascade (262144 points) and averaging it down to 8192 points as described in the text.

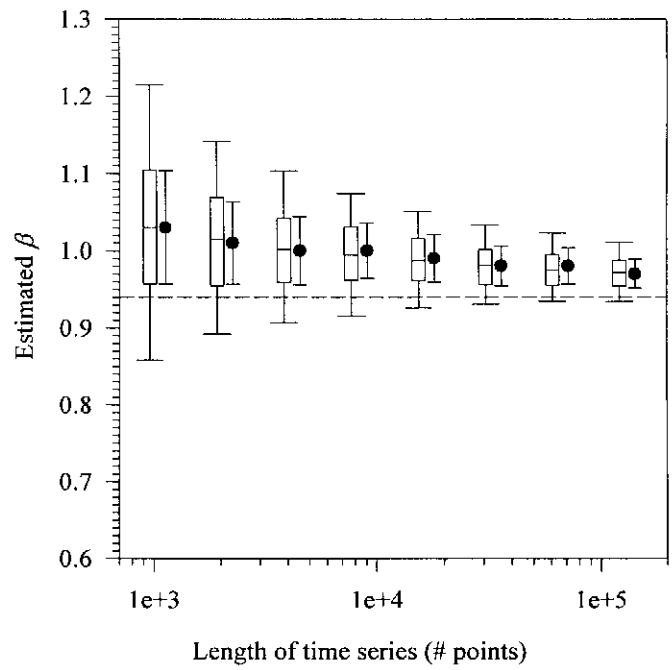

Fig. 5. A box plot of β estimated from 1000 time series for varying lengths computed using a log-normal cascade with σ = 0.2 so that the theoretical β = 0.94 (dotted line). The whiskers and boxes represent the 5, 25, 50, 75, 95 percentiles due to the sampling variability. The filled points with error bars represent the mean fit uncertainties.

The cascade is canonical and as long as $<W_0\text{-}1> = 0$ then $<W_k> = 1$. The cascade is bounded in the sense that as $k \to \infty$, $W_k \to 1$ and the variance of W_k decreases with scale in the following way for W_0 log-normally distributed:

$$<(W_k - 1)^2> = (<W_0^2> - 1)2^{-2(k-1)H} = (e^{\sigma^2} - 1)2^{-2(k-1)H}, \quad (15)$$

and so the variance goes to zero as $k \to \infty$.

As mentioned above the moment scaling of the absolute gradients of a bounded cascade generated in this way is reasonable over a finite range and is shown in Fig. 4. Since the scaling range in Fig. 4 is partial and midway between the entire range of scales, scaling right down to the smallest scales can be achieved by creating, say, an 18 step cascade (262144 points) and averaging the cascade back down to say 8192 points. An example of this is shown in Fig. 4 as well. $K_a(q)$ in (11) provides a good fit and can be used to estimate an effective σ to characterize $K(q)$ for the absolute gradients of multiaffine fields generated by (14). However, the estimated σ bears no analytical relation to the σ value used in (14) to construct the cascade.

3 Estimation Uncertainty

In the estimation of β and $K(q)$ there is an inherent degree of uncertainty resulting firstly from the accuracy of regressions or fit uncertainty (Fig. 1), and secondly the sampling variability. The latter arises from the fact that random realizations of the same process may yield slightly different estimates of β and $K(q)$. There is of course a dependence on how much data are used, and it is this relationship between estimate and time series length that is examined here for the estimates of β and $K(q)$.

The method used here is akin to the method to estimate confidence limits on estimated model parameters outlined in Press et al. (1992). In essence Monte-Carlo simulations of synthetic data sets are carried out with each data set being analyzed to obtain a distribution of a certain parameter such as β or σ.

3.1 Spectral Analysis

Sampling variability inherent in the estimation of β is investigated by generating 1000 realizations of a log-normal cascade with σ = 0.2 for various lengths of between 1024 and 131072 data and a theoretical value for $\beta = 1 - 0.2^2/\log(2) = 0.94$. Fig. 5 shows a box plot of the estimated values of β where the box and central lines are the quartiles and median value of β for the 1000 realizations. The whiskers represent the 5th and 95th percentiles. The filled points represent the mean estimated β and the error bars represent the mean fit uncertainty for the estimates of β. It can be seen from Fig. 5 that the fit uncertainties are of the same order of magnitude as the sampling uncertainties. It is apparent from Fig. 5 that of the order of 10^4 data points are required to estimate β to within ±0.1 at the 95% confidence level. For cascades of

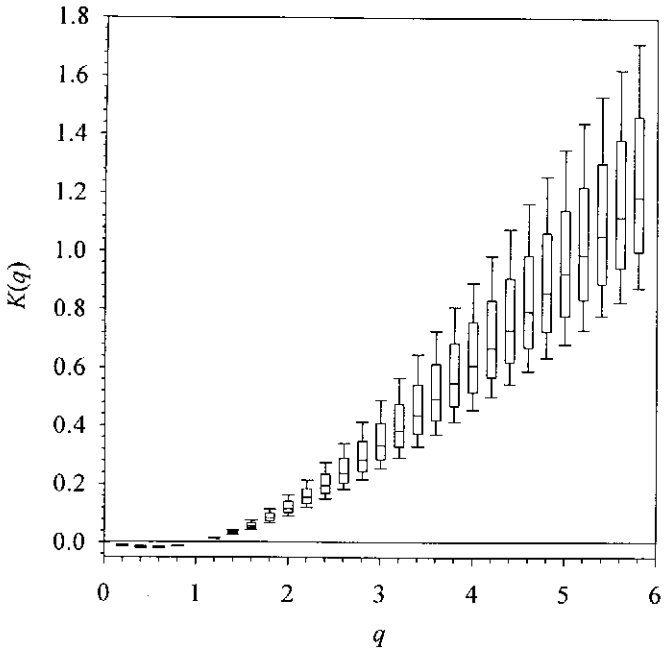

Fig. 6. Box plot for the sampling variability in $K(q)$ for 1000 log-normal 8192 point cascades generated with σ=0.3. The whiskers and boxes represent the 5, 25, 50, 75, 95 percentiles due to the sampling variability alone.

finite length, the estimated values of β are found to be biased from the theoretical β given by (12) as explained in the Appendix.

Since σ increases the variance of the generator, the variability of the time series increases with σ. An increase in this variability results in an increase in the sampling and fit. Increasing H for fixed σ had no effect on the absolute sampling uncertainty. Cascades with "fat-tailed" generators such as the log-stable (Schertzer and Lovejoy, 1987) cascade give slightly higher uncertainties particularly for low values of the Levy index, α. Microcanonical cascades yield smaller uncertainties than shown in Fig. 5 owing to their calmer nature.

3.2 Moment Scaling Analysis

The sampling variability in $K(q)$ is also estimated using 1000 realizations of a cascade with 8192 points. For each of the realizations, $K(q)$ is computed for a scaling range from 2 to 4096 points as the largest and smallest scales fluctuate and often deviate from the scaling behavior. The variability in $K(q)$ from sampling variability alone is represented by a box plot in Fig. 6. There is also a small degree of fit uncertainty in $K(q)$ for each point resulting from the uncertainty in the slope for each linear regression of the log-log scaling plots but this is insignificant by comparison with the sampling variability in Fig. 6.

From Fig. 6 it is evident that sampling variability in $K(q)$ increases rapidly for high order moments. In other words, the slope of $K(q)$ for high order moments, where $K(q)$ becomes increasingly linear, fluctuates strongly from sample to sample. This represents the sample variability in the relative magnitude of the few or single dominating value(s) present in each sample. Furthermore it is this variability which results in different values of q_{max} for each sample or realization.

Table 1. Ranked q_{max} estimates, for log-normal cascades with $\sigma = 0.3$ and therefore having $q_s = 3.9$.

Percentile	q_{max} (Method A)	q_{max} (Method B)
5%	1.5	2.2
25%	1.7	2.5
50%	2.4	2.7
75%	3.5	2.9
90%	5.8	3.1

The sample variability in q_{max} is illustrated by the two examples in Fig. 7. Fig. 7a shows a $K(q)$ curve computed for an 8192 point log-normal cascade generated with $\sigma = 0.3$. Since the data are simulated and contains no noise and zeroes, q_{min} is set to zero. q_{max} is estimated using the method (Method A in Table 1) described above in Section 2.2 in which the upper limit for q over which $K_a(q)$ is fitted is increased until such time that $K_a(q)$ exceeds the error bars for $K(q)$. This method, however, is not ideal and for the simulation studies $K(q)$ curves are computed for data sets where the quality of moment scaling is so good yielding very small error bars yet the curve becomes linear very quickly (i.e., low q_{max}). In this case because the error bars are so small, the very first $K_a(q)$ fit about $q \cong 1$ exceeds $K(q)$ by the uncertainty at $q \sim 1$. A degree of arbitrariness thus ensues in the process and it is useful if one can choose q_{max} to be the point where $K_a(q)$ exceeds $K(q)$ by two (or even three) uncertainties (i.e., 95% and 99% confidence limits). Fig. 7b shows a fit where q_{max} delimits the point where $K_a(q)$ exceeds $K(q)$ by twice the error bars shown. The process of arbitrarily relaxing the condition at which $K_a(q)$ is said to diverge from $K(q)$, is not serious in that it has little effect on the estimated parameter(s) from $K_a(q)$ (i.e., σ_{est} for the log-normal model). q_{max} is also estimated using the arbitrary criterion (Method B in Table 1) above where q_{max} is the q value for which the top 10% of the data contributes to 90% of the moment. Both methods give similar results and are tabulated in Table 1 for the example of 1000 log-normal cascades with $\sigma = 0.3$ and may be compared with the theoretical value computed using (13), $q_s = 3.9$.

Evaluation of the two methods, A and B in Table 1 and the use of the fixed value, q_s, considers the quality of the fit quantified by χ^2 and its probability of exceedence for each fit. Method A gave lower χ^2 values with χ^2 exceedence probabilities beyond the 95% limit for 70% of the realizations. Method B gave χ^2 exceedence probabilities beyond the 95% limit only 30% of the time. Using a fixed $q_{max} = q_s$ only provided similar fits only 20% of the time and furthermore increases the bias between σ_{est} and σ.

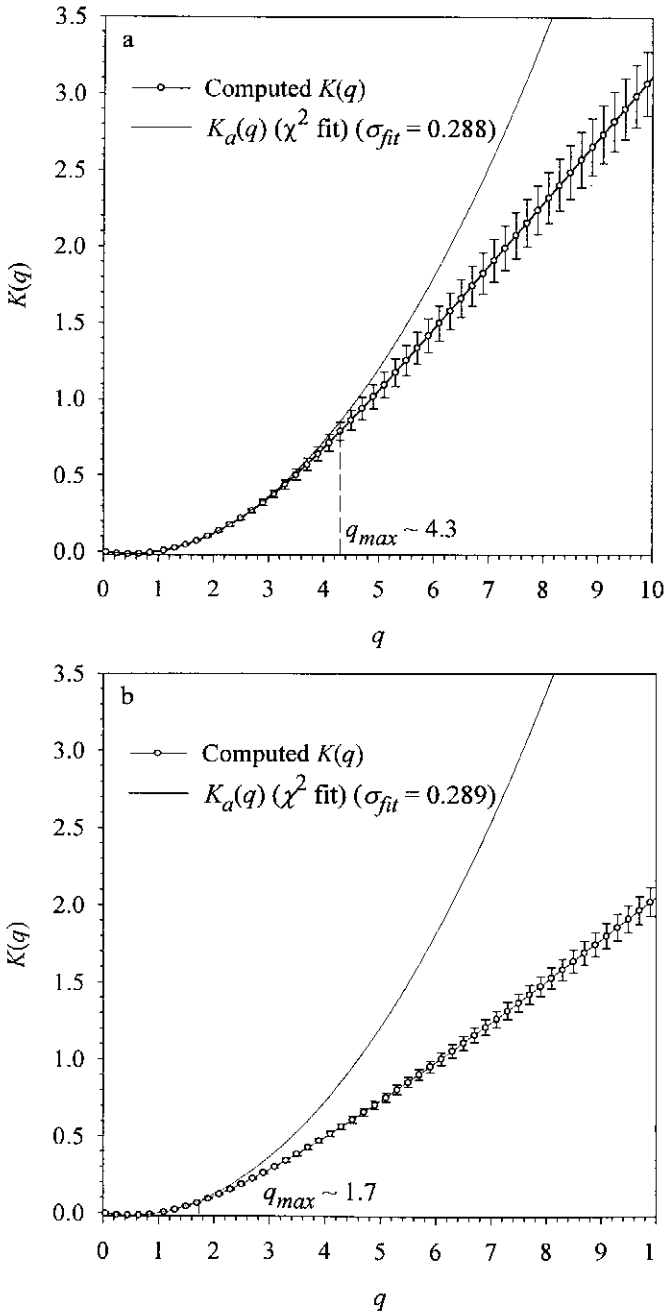

Fig. 7. Two different $K(q)$ curves for identical cascade processes. Both $K(q)$ curves result from 8192 point cascades generated with σ = 0.3. Error bars represent linear regression uncertainties in the slope of each log-log plot of the moment scaling which yields each value of $K(q)$. The fitted $K_a(q)$ curves are fit to $K(q)$ between q = 0 and $q = q_{max}$ where q_{max} is the point at which $K_a(q)$ exceeds the uncertainty at $K(q)$ (see text). For comparison, σ = 0.3 yields q_s = 3.9 using relation (13).

Using $q_{max} = q_s$ gives roughly the same results as using a more stringent criterion in Method B where q_{max} is the point where the top 5% of the data contributes to 95% of the q^{th} moment.

Neither Method A or B are ideal yet provide a rough estimate to q_{max} and more importantly reflect the notion of a variable q_{max}. As final notes on the estimation of q_{max}, there, firstly, did not seem to be a direct relation between the retrieved value, σ_{est}, and the value of q_{max} as one might expect. Secondly, there is no relation between q_{max} and the length of the cascade as already suggested by Schertzer and Lovejoy (1992).

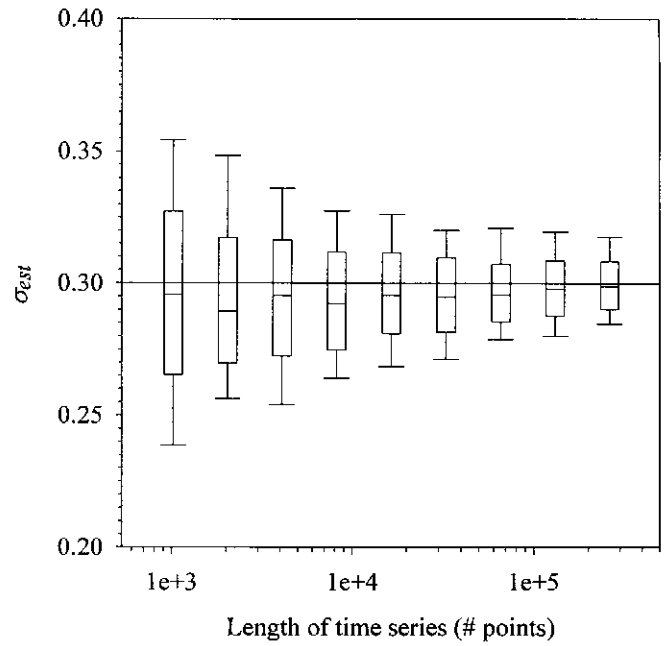

Fig. 8. Sampling uncertainty in the estimation of the generating parameter, σ_{est}, for single log-normal cascades of varying length simulated with σ = 0.3 as indicated by the horizontal reference line.

Fig. 8 shows the sampling uncertainty of the estimates of σ as a function of the number of points in each cascade. It is evident from this Fig. that estimates of σ have significant uncertainties and it is therefore difficult to estimate σ to better than 10% accuracy at the 95% confidence level. σ is estimated from $K(q)$ by a nonlinear fit of $K_a(q)$ in (11) to $K(q)$ from q = 0 to q_{max} where q_{max} is estimated using Method A above. By comparison, the fit uncertainty in σ for each realization is often less than 0.1% and so is negligible in comparison to the sampling uncertainty. Again, the bias is an artifact of canonical cascades as explained in the Appendix.

4 Mixing Differing Random Processes

While the previous section suggests obtaining results from very long time series in order to reduce uncertainty, some simple tests presented in this section illustrate the importance of avoiding taking time series so long that they include different processes. Mixing processes or, in other words, including physically different meteorological processes (e.g., stratiform frontal rain and convective rain) in a single time series may result in one of the processes dominating all of the statistics. The necessity to be careful when mixing different processes has been suggested in the literature (Lovejoy and Schertzer, 1991, p. 138).

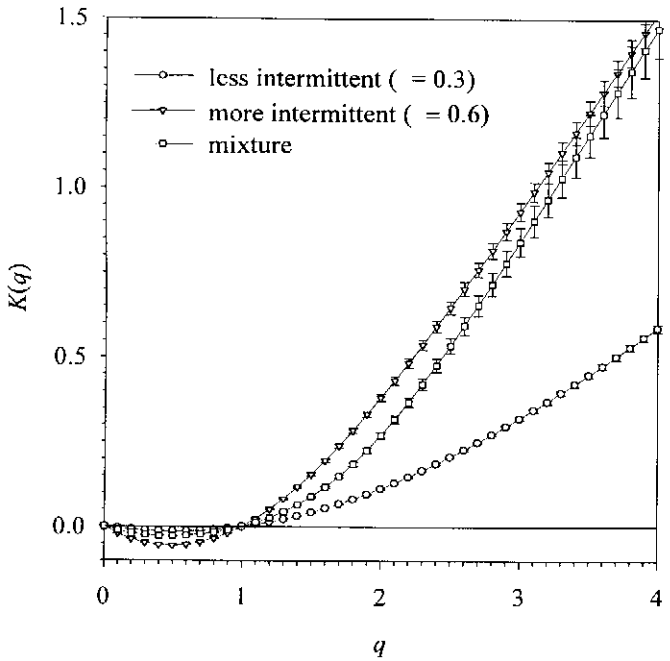

Fig. 9. $K(q)$ curves for two differing multiscaling processes and the mixture of the two. q_{max} values were estimated to be 3.0, 1.5, and 2.0 for the less intermittent, more intermittent and mixture $K(q)$ curves, respectively.

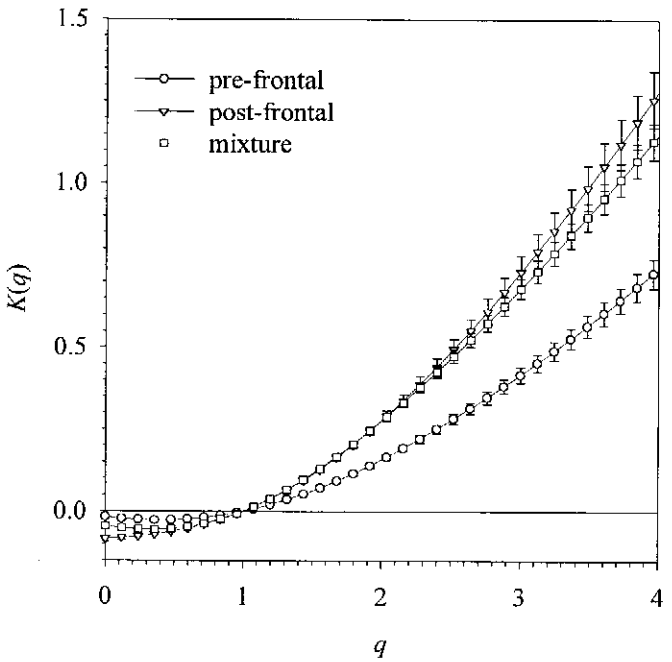

Fig. 10. $K(q)$ curves for pre-frontal and post-frontal rain as well as the mixture of the two. Estimated q_{max} are 2.3, 2.1, and 1.9 for the pre-frontal, post-frontal and mixture $K(q)$ curves, respectively.

4.1 Simulation Studies

By simulating a number of cascades with different $K(q)$ curves and mixing different proportions of them together in an ensemble, one can examine what the resulting β values and $K(q)$ curves are for different proportions of processes. Consider a mixture consisting of two log-normal cascades with half of the data constructed with high σ (more intermittent) and the other half with low σ (less intermittent). While theoretically such a mixture should destroy scaling all together, mixtures of cascade simulations often have excellent scaling for all moments albeit with a reduction in the upper limit of the scaling range. Even the reduction in scaling range was inconsistent and highly variable. Fig. 9 illustrates the resulting $K(q)$ for such a mixture and comparison is made to the individual $K(q)$ curves for each half. In this example the less intermittent half has a mean that is twice that of the more intermittent half yet, clearly, the scaling of the mixture is dominated by the more intermittent statistics. This is explained by comparing the higher order moments ($q \geq 2$) of the two halves which shows that the more intermittent data outweighs the less intermittent data by a factor of three for $q = 2$ and a factor of 35 for $q = 3$. In this particular example the scaling range for the mixture is reduced to ~3 orders of magnitude from ~4½ orders of magnitude for the individual halves. q_{max} values quoted in Fig. 9 are estimated using Method B). In general the domination of one signal over an other is determined by a combination of the intermittency and their relative strengths. If the less intermittent signal in the example above is sufficiently stronger relative to the more intermittent half, it is possible to have the less intermittent signal dominating all moments.

4.2 Mixing Data from Pre-frontal and Post-frontal Rain

The data set discussed here consists of ~68 hours of rain gauge data during which a front has passed roughly half way through the time series. The pre-frontal conditions consisted of a blocked warm air flow with near neutral stability for ~34 hours leading up to the front. The post-frontal conditions consisted of an unstable and cooler air mass. These assertions are supported by MSL pressure analyses, numerous soundings (temperature, pressure, and humidity), hourly meteorological station data, and ground based cloud observations. Details are contained in Purdy (1997). The pre-frontal rainfall was ~6.3 mm/hr on the average compared with ~1.9 following the front.

All case studies analyzed here use data from high resolution electronic rain gauges which function by generating constant sized drops at the bottom of a 15 cm diameter funnel collecting the rain. The drops are sensed by an electronic probe and tallied digitally. One generated drop is approximately equivalent to $1/160^{th}$ of a millimeter of rainfall, and over an integration period of 15 seconds this represents a resolution of ~1.5 mm/hr. Longer integration periods improve this resolution proportionately. See Stow et al. (1997), Austin (1994), Hosking et al. (1985), and Harris et al. (1996) for more information about this rain

gauge. All the data used was collected in early November 1994 on the South Island of New Zealand.

β and $K(q)$ are computed before and after the front as well as for the mixed time series consisting of both pre-frontal and post-frontal rain. The time series is multiaffine both before and after the front and β is marginally smaller for the pre-frontal data. Taking gradients and finding $K(q)$ produces the curves shown in Fig. 10. The $K(q)$ curve for the pre-frontal rain is shallower than $K(q)$ for the post-frontal data. As in Section 4.1, it is not surprising that the mixed time series featured a $K(q)$ dominated by the portion of the time series with the steeper $K(q)$, which in this case was the post-frontal rain.

The data used for Fig. 10 scales well between time scales of 2 minutes to 4¼ hours (2½ orders of magnitude). Higher order moments ($q > 1$) scale well down to 15 seconds (3 orders of magnitude) suggesting the effect of rain gauge quantization in lower order q (see below, Section 5.1).

The $K(q)$ for these time series also show $K(0) \neq 0$ as a consequence of the presence of zeroes in the time series. Again, while some of the zeroes are an artifact of the gauge (see below) some may be real. The result is a $q_{min} > 0$ below which $K_a(q)$ for a cascade (without an atom at zero) will not apply. The $K(q)$ are poorly fit by the log-normal model in (11) and suggest using another model such as the log-stable model (Schertzer and Lovejoy, 1987).

5 Effects of Noise and Instrumental Artifacts

In this section the effects on analysis results of noise and instrumental artifacts are examined empirically by modeling these effects on cascades. Since the specific details of the types of noises and artifacts which may be of concern to the user of a particular instrument are too numerous and varied to be included, only three general effects are considered here. The first effect has been briefly mentioned in the previous section and is referred to as quantization noise. Quantization is an artifact of one of the most common types of rain gauges today, the tipping bucket rain gauge, and has an impact particularly at low rain rates. For this reason, this effect is also referred to as the tipping bucket effect. The electronic gauges used in this study are in some sense tipping bucket gauges as well, except that the 'bucket' is a single drop of water generated by the nozzle assembly. The second effect is referred to as additive noise and for the purposes of illustration restricted to Gaussian white noise. In practice a noise added in this way could be, for instance, representative of electrical or background noise in such instruments as impact disdrometers, and other electrical devices such as the sonic gauge (Duncan, 1993; Fabry, 1996). More important to this study, as will be shown below, is the fact that the aforementioned quantization effects behave significantly like high level additive noises following a gradient transformation. Gradient transformations are the third

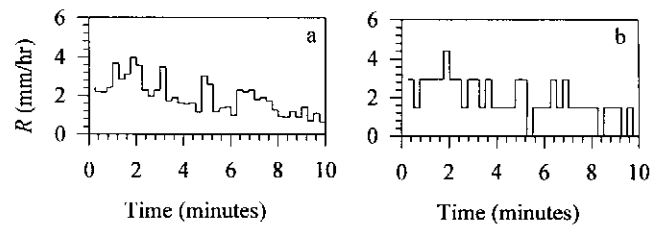

Fig. 11. The tipping bucket effect at low signal levels. A rain rate, R, time series at 15 second resolution simulated by a log-normal cascade in (a) on the left is recorded as (b) by an instrument with a 'bucket' size equivalent to $1/160^{th}$ mm equaling a quantization of 1.5 mm/hr in 15 seconds.

effect studied here although they not really an instrumental artifact or noise, but a consequence of the analysis procedure. $K(q)$ is shown to be robust to the addition of small amounts of noise or quantization but the effects of additive noise or quantization are greatly enhanced if one takes gradients of the field prior to calculating $K(q)$ as is routinely done for multiaffine fields.

5.1 Quantization: the Tipping Bucket Effect

A tipping bucket rain gauge records the time taken to accumulate a unit of rainfall, usually around 0.1-0.2 mm. It is difficult to deal with a series of data which has a variable time step and it is therefore convenient to convert the data to one with a fixed time step. The electronic drop counting gauges used in this study work by accumulating the rainfall into drops of known volume and then logging the number of these drops passing through the gauge per unit of time. This has the advantage of directly producing a time series with a fixed time step. The data from such a gauge will be quantized with a quantization level equal to the rain rate that corresponds to one drop generated per unit time. For the gauge data used here the quantization level is ~1.5 mm/hr at 15 second resolution. The mean rain rate given that is raining is often in the 1-5 mm/hr range and therefore the quantization effects are significant for high time resolution measurements of light rain.

The tipping bucket effect is quite different to the quantization associated with the digitizing of a signal. For low rain rates, a signal below the resolution of the digitizer would be set to zero, whereas the gauge accumulates these low signal levels and then records a pulse when enough rain has accumulated to fill the bucket (or form a drop in the case of the electronic gauge used here and described above). This effect is illustrated in Fig. 11.

The effect of the tipping bucket effect on spectra of time series is shown in Fig. 12. In short the effect is to introduce a flattening of the tail or a sharp 'kink' in the high frequency end of the spectrum. It is similar to the effect of additive noise below except for the sharper break in scaling with little effect on the exponent of the spectra for frequencies lower than that kink and the estimate of β is

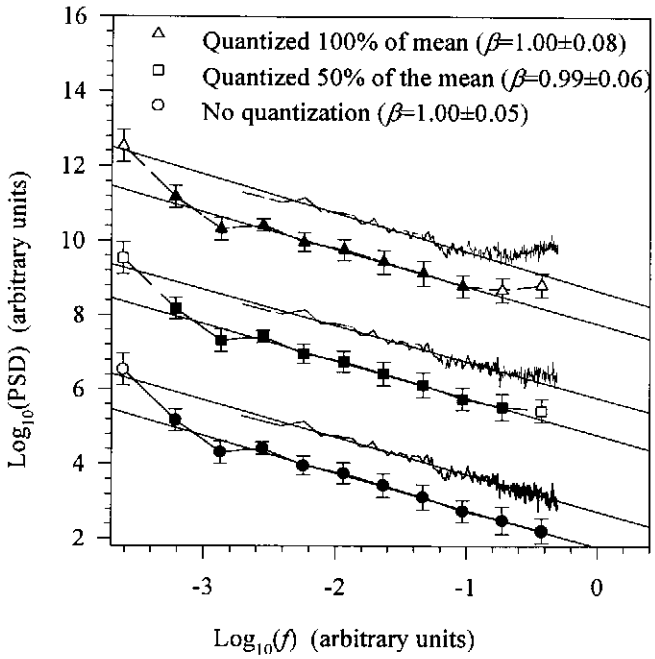

Fig. 12. Effect of tipping bucket quantization on time series spectra generated by 8192 point log-normal cascades with σ = 0.2. The regressions for the spectra with noise do not include data in the last octave and last two octaves for the 50% and 100% cases, respectively.

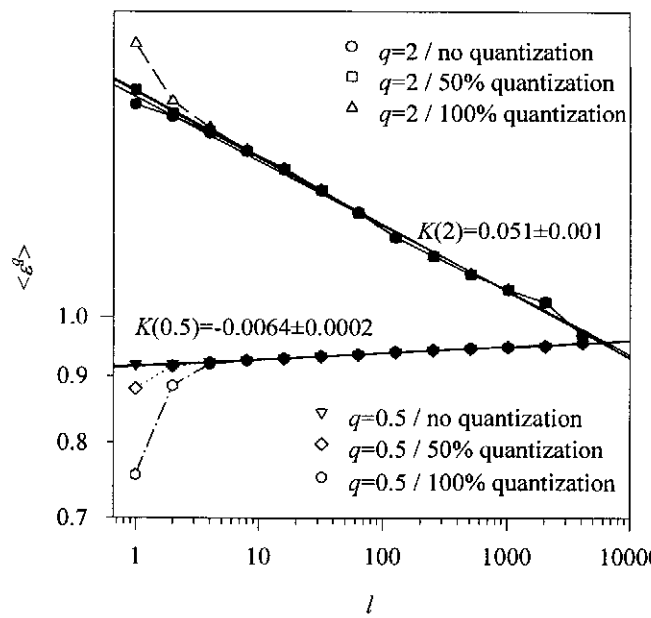

Fig. 13. The effect of quantization on scaling moments.

hardly affected. The level of quantization is defined by the fraction of the mean signal level and referred to in Fig. 12 as a percentage. To put the apparently high values of quantization in perspective, consider a rain gauge time series where the rain rate resolution of the gauge is 1.5mm/hr (based on the electronic gauge described above). A mean rain rate of 3 mm/hr would mean having a quantization level of 50%.

The tipping bucket effect on moment scaling is shown in Fig. 13. As expected there is a scale break at small scales due to the quantization. This break is seen more pronounced for the lower order q. This is a consequence of the fact that low signals are enhanced by low order moments and it is the low signals that are also more affected by quantization as illustrated in Fig. 11. For very low q ($q \approx 0$) scaling range can be significantly reduced, if not destroyed altogether, and introduces a $q_{min} > 0$.

In measured rainfall records where there may be long periods of zero rainfall (which, of course, requires an independent assessment), it should be noted that the quantization level should be estimated relative to the conditional mean rainfall (i.e., rainfall given that it is raining).

5.2 Additive Noise

As a simple but illustrative example of the effect of additive noise on multiscaling analysis, white Gaussian noise is added to cascades. The noise level is described in the usual way by the signal to noise ratio (SNR) defined as the ratio of the mean squared rainfall to the mean squared noise (i.e., $<R^2>/<N^2>$), or more conveniently by its inverse expressed as the noise percentage. The noise distribution has a mean near zero and is truncated so as not to end up with negative rainfall. Fig. 14 shows the effect on power spectra of adding noise with powers up to 30% of the signal power. From these spectra one notices a gradual flattening of the high frequency end of the spectra and a decrease in the value of β with increasing noise. The values shown for β are computed only from the octave binned spectra. Compared to the sampling and fit uncertainties for a field of this length, the observed decrease in β is seen to be significant and greater than the estimated uncertainty in β for the high noise (30%) case. However, β seems fairly robust to the addition of small amounts of noise. With the addition of noise the tails for $f/f_{samp} > 0.1$, (f_{samp} is the sampling frequency of the signal) introduce an artificial break in the scaling, and so are not included in the regressions to estimate β. The effect of additive noise on multiaffine fields is similar.

Fig. 15a shows the scaling of the 2nd moment for various degrees of contamination by Gaussian white noise. The increase in t_{min} and therefore the reduction in scaling range is evident. Clearly, if the noise level is high enough (exactly how high depends on the statistics of the field being studied) the scaling range will be sufficiently small that the data ceases to be multiscaling. All moments displayed the same small scale behavior and slight decrease in slope. The smaller scales, indicated by the white points, are excluded from regressions as for the estimate of β. One also notices that while β decreases so does $K(2)$ which

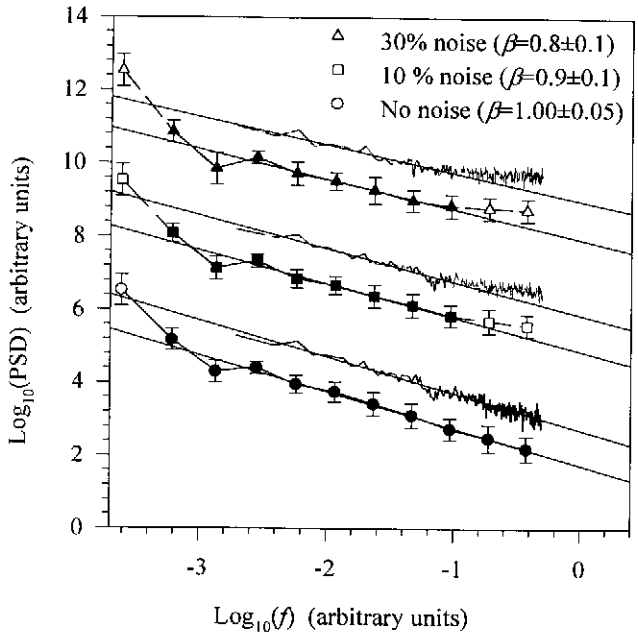

Fig. 14. Effect of additive noise on time series spectra. Each spectra is computed from the same 8192 point log-normal cascade (with $\sigma = 0.2$) but with different noise levels indicated on the legend. For each octave binned spectrum there is a corresponding line spectrum computed using the subdivision method of noise reduction.

means that noise exacerbates the breakdown in the relation, $\beta = 1 - K(2)$, for multiscaling fields.

The effect of noise on the estimate of $K(q)$ is seen in Fig. 15b. In general, $K(q)$ becomes less steep with the addition of noise. Equally striking is that the low order moments are the most strongly affected by noise. The high noise (30%) case is sufficient to greatly alter $K(q)$. The lower noise (10%) case seems to be very similar to its noise free counterpart pointing again to the robustness of $K(q)$ to the addition of small amounts of noise. It is worthy to note, however, that the fitted model, $K_a(q)$ (dotted line) underestimates $K(q)$ of the 10% noise case for higher order q. This is explained by the fact that the high order moments (reflecting the statistics of higher fluctuations) are insensitive to the generally low level noise. However, the fitting is still influenced, to a significant degree, by the low order moments. The estimated values, σ_{est}, parameterizing the log-normal $K_a(q)$ are σ_{est} = 0.28, 0.24, 0.17 for the noise free, 10% noise, and 30% noise data, respectively. The q ranges over which the fits are taken also change significantly. The noise free data has q_{min} = 0, and q_{max} = 2.8, while the data with 10% noise has q_{min} = 0.7, and q_{max} = 1.8 and for the high noise data, q_{max} drops to 1.5.

5.3 The Effect of gradients

The process of taking gradients as defined in (4) is a consequence of the analysis and not the measuring

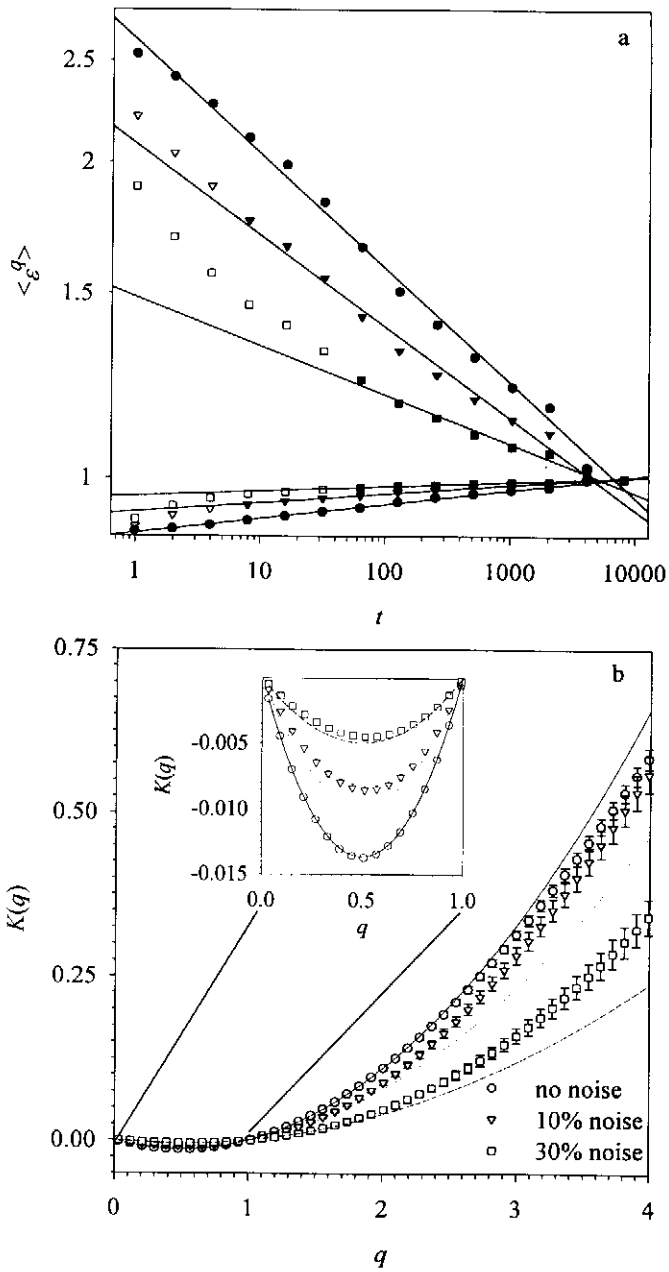

Fig. 15. Effect of additive noise on moment scaling. (a) The effect of noise on the scaling of the $q = 2$ (negative slopes) and $q = 0.5$ (positive slopes) moments for a cascade with no noise (circles), 10% (triangles) and 30% (squares) additive white Gaussian noise, respectively. (b) The effect of noise on the $K(q)$ function for various levels of noise contamination. All curves are computed from the same 8192 point log-normal cascade ($\sigma = 0.3$). The inset shows that even small amounts of noise affect the lower order moments ($q < 1$).

instrumentation. When studying the effect of the noises above on multiaffine fields it was found that the act of taking gradients strongly enhances the adverse effects of these noises. Examples of the enhancement are listed in Table 2 in which figures are computed by separating out the noise (additive or quantization) and monitoring their levels separately before and after gradients of the field. Because rainfall is non-negative, the amplitude of the noise

Table 2. Examples illustrating the enhancement of noise due to taking gradients of a multiaffine field constructed using a bounded cascade with $H = 0.3$ and $\sigma = 1.4$.

Noise	Noise Percentage (Field)	Noise Percentage (Gradient Field)
10% additive	10%	101%
30% additive	30%	304% *
50% Quantization	0.3%	7%
100% Quantization	0.9%	22% *

* Moment scaling destroyed

free signal decreases when taking absolute gradients. However, the noise is not non-negative, and therefore taking absolute gradients is the same as adding uncorrelated noise which increases the noise variance.

The addition of white noise or quantization of a (multiaffine) field followed by taking gradients results in a new field which can be represented as the noiseless gradient field plus an effective additive noise referred to here as gradient noise. This effective gradient noise has a flat spectrum below a certain frequency and has a scaling spectrum ($\beta > 0$) above that frequency. For the examples in Table 2, the addition of white noise followed by taking gradients results in a noise which has $\beta \approx 0.9$ for $f/f_{samp} > 0.1$, where f_{samp} is the signal sampling frequency. For the case of quantization, the gradient noise has $\beta \approx 2.9$ for $f/f_{samp} > 0.3$.

As indicated in Table 2, the case of 30% noise results in ~300% gradient noise and destroys scaling altogether. In the case of 100% quantization, the scaling range following gradients was reduced to less than two orders of magnitude which can hardly be considered as scaling. In the other cases, the scaling range was reduced from well over two and a half orders of magnitude down to just over two orders of magnitude.

The resulting $K(q)$ curves are shown in Fig. 16. Moments less than ~0.3 were found not to scale for the data with noise or quantization and for the case of quantization, $q_{min} \approx 0.7$. As in Section 5.2, the scaling of the lower order moments changes most with the addition of noise or quantization and influence the fitting of a model $K(q)$. Once again, models underestimate $K(q)$ for large q, although only marginally for the case with 50% quantization. q_{max} for the noise free data was low in this example with $q_{max} \approx 1.5$. the estimated parameters, σ_{est} for the log-normal model were 0.35, 0.16, and 0.30 for the data with no noise, 10% additive noise and 50% quantization respectively. Again, $K(q)$ seems fairly robust to quantization but only for $q \approx 1$ and above if gradients are taken.

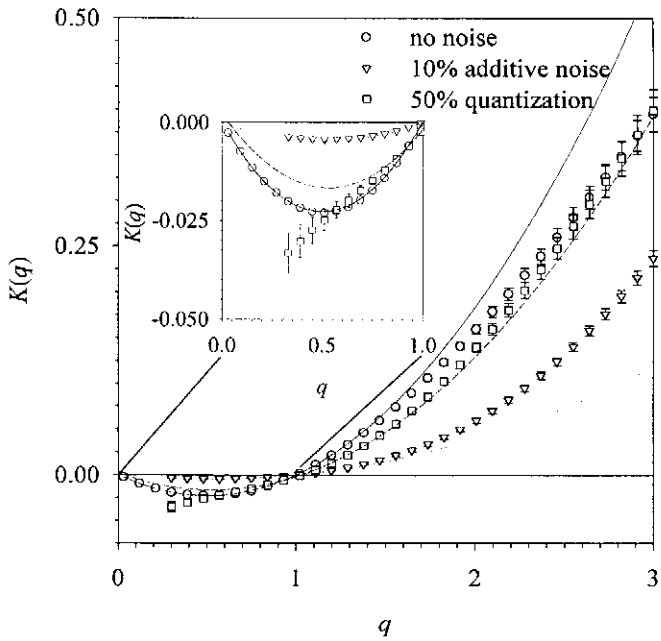

Fig. 16. Effect of quantization on $K(q)$ after gradients. The time series used to compute the curves were simulated by a dressed 8192 point log-normal bounded cascade with $\sigma = 1.4$ and $H = 0.3$. The inset enlarges $K(q)$ for $q \leq 1$. The contaminated data do not have scaling gradients for moments less than $q \approx 0.3$ and is the reason for the truncated $K(q)$ curves.

5.4 Effect of Spurious Spikes

In 1994 on November 4th, a time series was collected with a possible 'glitch' likely to be an instrumental artifact. Another nearby rain gauge a few kilometers away recorded very light rainfall during the same period, but the short and intense spike shown in Fig. 17 is too sudden and lacks any "lead-up" and "wind-down" to the peak rain rate suggesting that it may be a build up of water in the gauge funnel followed by a quick surge perhaps lasting some 15-30 seconds. The series in Fig. 17 was combined together with the series of the nearby gauge to form an ensemble of two series of 8192 points so as to examine the effect of this glitch on the estimation of β and $K(q)$.

The effect of the glitch on the power spectrum is seen in Fig. 18. The top two plots represent spectra for the data with the glitch and the bottom two curves are for the data without the glitch. Since the glitch actually comprises of 33% of the total combined power of the signals, it is not surprising that it has a noticeable effect. Furthermore, the glitch also dominates the quantization effect that is so obvious in the bottom two spectra for the data without the glitch. The flat noise tail in the two bottom spectra are due to quantization noise which is estimated to be at a level near 300% of the mean rainfall from 16 to 32 hours in Fig. 17.

Although $\beta \sim 1.2$ for the series without the glitch, the moments are found to scale without the need for gradients and is thus a multiscaling field. This is fortunate since the high quantization would have a detrimental effect on $K(q)$ estimation following a gradient transformation. The moment scaling range over moments from $q \approx 0.2$ and greater was approximately three and two and a half orders of magnitude for the cases with and without the glitch,

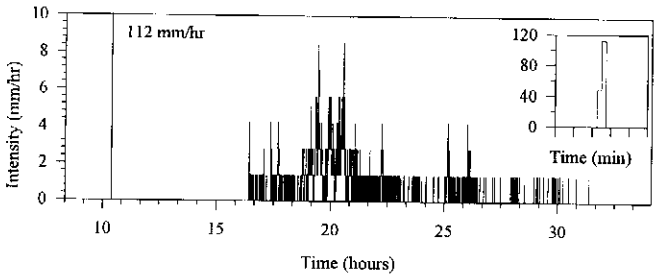

Fig. 17. Sample Rain rate time series at 15 second resolution recorded November 4th, 1994 on the South Island of New Zealand. The inset is an expansion of 5 minutes during the 10th hour of the time series during which the glitch occurred. There was no rain in the first 10 hours of this 8192 point series.

respectively. The magnitude of the discrepancy in the apparent breakdown of relation (12) between β and $K(2)$ is large here but discrepancies even larger than this can be reproduced using simple (noise free) canonical cascades.

The $K(q)$ for the data with and without the glitch are shown in Fig. 19. The difference is large primarily for $q >$ 1 which may cause differences in the estimation of the curvature parameters of a $K(q)$ model such as α in the log-stable model (Schertzer and Lovejoy, 1987).

5.5 A High Resolution Rain Gauge - Radar Comparison

Comparing data from two instruments as different as a rain gauge and a radar is a non-trivial task. Radars and rain gauges have very different sampling statistics and the conversion of radar reflectivity (Z) to rain rate (R) incorporates nonlinear transformations. There is a large literature on Z-R relationships (e.g., Atlas, 1990 and references therein; Smith and Krajewski, 1993) which discuss errors due to sampling volume discrepancies, short term changes in drop size distributions, and up drafts. It should be noted, however, that the data analyzed here are unusual in that the wind speeds at the ground were exceptionally light thus minimizing some of these problems.

On the 18th to the 19th of October, 1996, a low pressure system to the south west of New Zealand was blocked by a high pressure system over New Zealand's North Island resulting in a light westerly flow over the South Island producing rain on the west coast of the South Island in near constant atmospheric conditions. Simultaneous rain gauge and vertically pointing radar (VPR) time series at 15 seconds resolution were collected over ~34 hours (8192 points) during the period and are analyzed and compared here. The electronic gauge (also used above) had an enlarged funnel resulting in an exceptionally low quantization level of 0.34 mm/hr at 15 second resolution for this. The VPR time series is sampled at 500 meters where the beam width is 13 m and the pulse height is 60 meters resulting in an illuminated volume of approximately 8000 m^3. Each 15 second measurement is

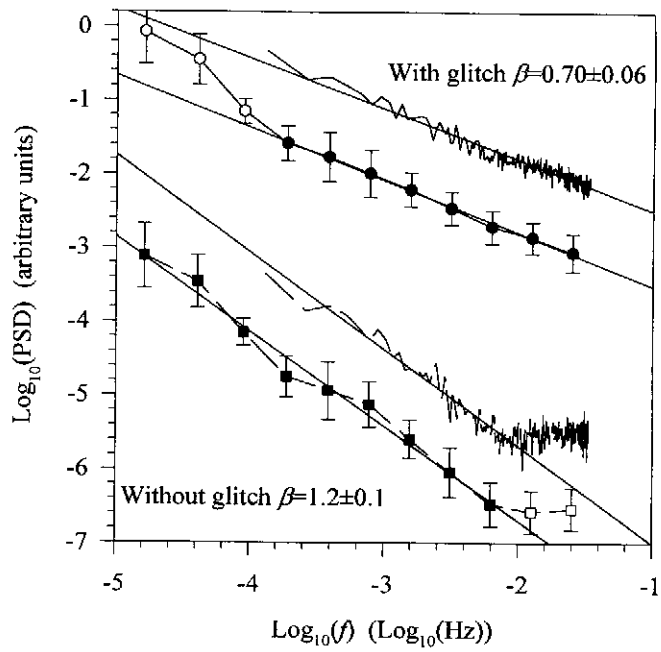

Fig. 18. The effect of possible glitches on the power spectrum of rainfall time series of 8192 points in length. The top curves are the average and octave binned power spectra of the time series with the 'glitch' and have the combined β shown. The bottom two plots are for the same combined time series with the glitch removed. The bottom two regressions are for $f/f_{samp} < 0.01$ Hz. The spectra are an ensemble of two nearby gauges only one of which has the glitch shown in Fig. 17.

the result of just under 4000 pulses. The two time series are shown in Fig. 20 where a 2½ minute delay (obtained by maximizing the cross-correlation between the series) has been added to the rain gauge time to account for the delay in the rain dropping 500 meters to the gauge and the delay of the flow of water through the gauge itself. The rain gauge mean is 5.44 mm/hr giving a very low quantization of 6%. With hindsight of the analysis results below, the VPR rain rate was computed using a Z-R relation of the form $Z = aR^b$ with b chosen to be $b = 1.7$ which provides conservative estimates of peak rainfall rates (e.g., Seed et al., 1996). Since a is effectively a normalization constant, it has no bearing on the results of multiscaling analysis, yet a value of $a = 94$ results in a mean equal to the rain gauge mean. Least squares regressions of the VPR Z measurements versus the rain gauge R measurements resulted in $b \approx 1.4$ which would enhance the differences seen in Fig. 20. Visual comparison of the two series suggests a significant correlation between the two (correlation coefficient $r = 0.65$). The most noticeable difference is the larger maximum to mean ratio for the VPR series however sometimes the reverse is true particularly in the last six hours of the time series.

The spectra for the two series are similar with $\beta = 1.48$ and $\beta = 1.38$ for the gauge data and VPR derived rain rates, respectively. The moment scaling range is slightly better for the VPR derived rain rates with scaling from 30 seconds to 8.5 hours (over 3.5 orders of magnitude) while the

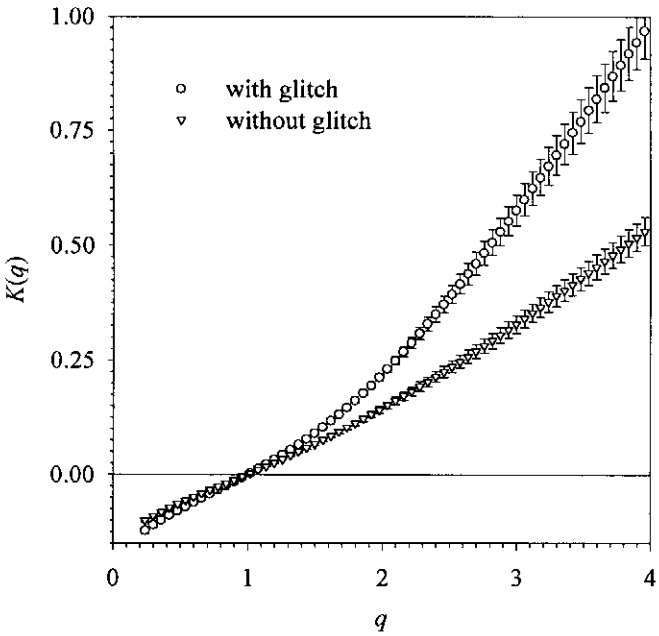

Fig. 19. Effect of the glitch in Fig. 17 on $K(q)$ for rainfall series of 8192 points in length. The scaling ceases for moments below $q \approx 0.2$ as a consequence of the high degree of quantization at small scales.

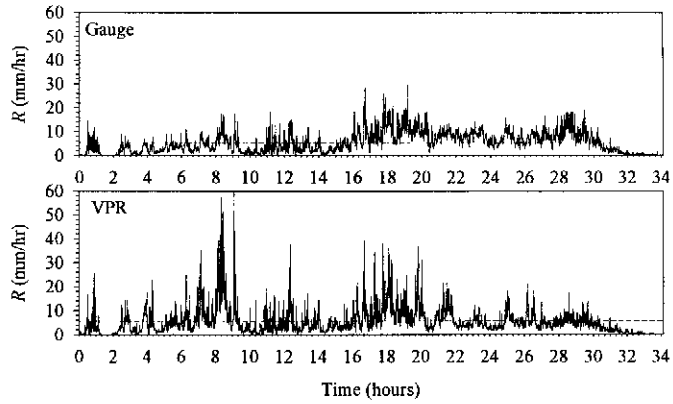

Fig. 20. Simultaneous rain gauge and VPR time series. Each series is 8192 points long and the VPR series results from radar reflectivity averaged over 15 seconds in time and between 500 and 560 meters directly above the gauge. Reflectivity is converted to rain rate, R, using $Z = 94R^{1.7}$. The horizontal dashed lines indicate the means of the signals which are the same for the two series and equal to $\langle R \rangle = 5.44$ mm/hr.

scaling range for the rain gauge is from 2 minutes to 8.5 hours. The resulting $K(q)$ curves are shown in Fig. 21. The difference in intermittency suspected from visual comparison of Fig. 20 are confirmed here. q_{max} for the curves are estimated, using Method B above, to be approximately 2.5 and 3.5 for the VPR and rain gauge data, respectively. Because b in the Z-R relation used to derive the rain rates for the VPR was chosen to be high, the observed difference between the two $K(q)$ in Fig. 21 represent a minimum discrepancy. A lower value of b would enhance the VPR intermittency even further.

The comparatively greater intermittency for VPR derived rain rates is a somewhat surprising result when one considers the difference in sampling area of the two instruments. The gauge has a diameter of 0.2 m while the VPR has a beam diameter of 13 m and to make a very rough estimate of the vertical scale one may consider that over 15 seconds rain may move ~75 meters (based on ~ 5 m/s average drop speed) which is comparable with the 60 meter pulse height. From these differences sampling alone suggests the radar sampling volume is much larger and so should be smoothed out more than the gauge, however the reverse seems true.

There are a number of factors to consider in hypothesizing why this may be. Firstly, the fact that while the VPR data had peak values which generally exceed the gauge peak values (relative to their respective means), sometimes the reverse is true and this suggests variability in the true Z-R relation (Smith and Krajewski, 1993), which of course is unknown. Z-R variability may be the result of changes in drop size distribution with time and/or changes in updraft or down-draft velocity with time. Given the light wind speeds (typically less than 3 km/hr), the latter is unlikely. The light winds also suggest that underestimation of the gauge due to horizontal advection (e.g., Rodda, 1971) is not likely to be occurring.

Considering that the reflectivity is very well measured (~4000 pulses/measurement) radar accuracy is not a likely cause for the discrepancy. The limited evidence at this point suggests that changes in time of the drop size distributions may be the only plausible hypothesis. In particular the most significant deviation between the radar and gauge occurs during the 8th hour where differences in the drop size spectrum (in this case, tending to an increase in larger drops) could explain such a deviation. Physically, the discrepancy is difficult to explain with the limited information given. This issue requires further examination with the possible help of additional instrumentation such as drop size spectrometers. Such a project is currently underway.

6. Summary and Conclusions

Multiscaling techniques provide a method to quantitatively characterize the intermittency and smoothness in rainfall and other highly variable geophysical fields. Rainfall brought on by different meteorological processes show differences in the multiscaling parameters as shown in Section 4.2 and Harris et al. (1996). The aim of future work with these methods will be to investigate links between the multiscaling properties of rainfall and the meteorology producing the rain.

Before differences in estimated scaling parameters can be used to reflect differences in meteorological processes, it is important to examine the accuracy and robustness of the analysis results. In this paper, multiscaling analysis is restricted to the computation of the spectral scaling exponent, β, and the moment scaling exponent, $K(q)$. The

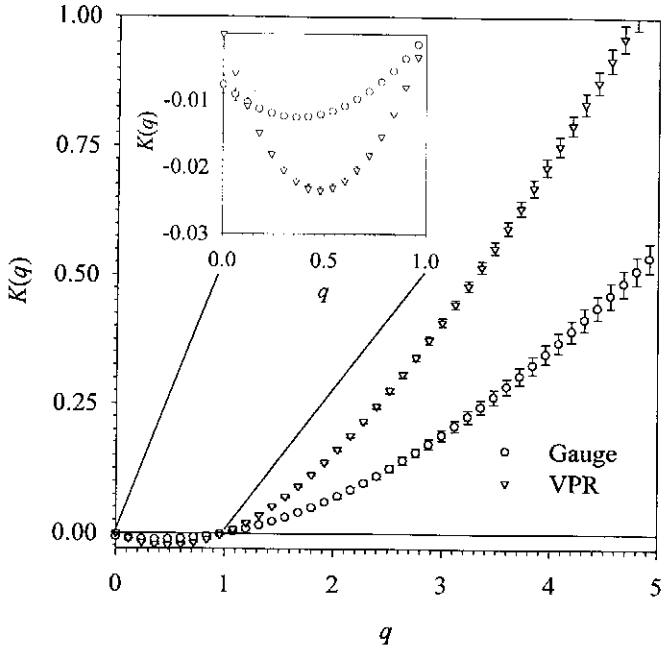

Fig. 21. $K(q)$ functions from simultaneous rain gauge and VPR derived rain rate time series. The inset enlarges the $K(q)$ curves for $0 \leq q \leq 1$. The presence of zeroes in the rain gauge time series partly due to the small amount of quantization results in $K(q) \neq 0$. q_{max} for the curves were estimated to be $q_{max} \approx 2.5$ and 3.5 for the VPR and gauge curves, respectively.

three principal issues concerning multiscaling analysis which are addressed in this study are 1) field sampling variability, 2) results of mixing physically different fields, and 3) the effects of instrumental artifacts. These issues are primarily studied using simulations and in some cases further illustrated with real data.

Canonical cascades are used to study the sample variability in estimates of β and $K(q)$. The magnitude of the variability may be contributed to in part by the fact that canonical cascades are known to have high sample variability (Mandelbrot, 1974). In this case the method of estimating sample variability by Monte Carlo simulations of canonical cascades puts an upper limit on the sample uncertainty of multiscaling fields. The extreme sample variability in $K(q)$ for high q is argued to be a consequence of the random occurrence (or absence) of extreme values. This is reflected by the random nature of a maximum moment, q_{max}, above which the $K(q)$ curve becomes increasingly linear. Because this transition to linearity is gradual, estimation of q_{max} is difficult. The two methods used here are not ideal yet offer conservative estimates of q_{max} which seem to minimize bias and χ^2 when fitting analytical forms, $K_a(q)$. The methods are based upon: A) fitting a form, $K_a(q)$, to the estimated $K(q)$ over a small range about $q \approx 1$ and progressively increasing the q range until $K_a(q)$ departs from $K(q)$ by a certain amount. B) Establishing a simple criterion where q_{max} is considered to be the moment where the highest X% of the data values contribute to Y% of the moment. Method A leaves doubts as to its robustness (occasionally returning unusually low q_{max}) but has the advantage that it can be used to estimate q_{min} below which $K(q)$ is dominated by noise and/or zeroes or simply fails to suit a particular model. In this case, q_{min} and q_{max} empirically define the range of q over which a model, $K_a(q)$, applies to the data. Method B has the advantage that it is not model dependent and relates q_{max} more directly to the numerical reason for which $K(q)$ becomes more linear (i.e., $K(q)$ is determined by very few of the data points). Method B's drawback is that the criterion is somewhat arbitrary yet so are so many statistical criteria. Good results were obtained using X% = 10% and Y% = 90%. Estimation of q_{max} using either method were generally lower than the theoretical estimate, q_s, (Schertzer and Lovejoy, 1992). This essentially amounts to the estimates of q_{max} used here being more conservative than q_s. In reality there is no specific q at which $K(q)$ becomes linear, but rather a range of q in which the change occurs so it is difficult to say where in this range one should designate q_{max}. The authors regard this as a problem which requires more thought yet the simple (yet non-ideal) empirical methods proposed above clearly emphasize that the estimation of q_{max} and q_{min} should be realization dependent rather than a fixed value for all similar processes.

Recent efforts have been made particularly in the hydrometeorological community to link physical processes with the statistical structures they produce. If progress is continued to be made towards this goal, efforts must be made to use whatever knowledge available of the physical state of the process creating a data set. As demonstrated above, the combination of different physical processes into a single data set for analysis can have detrimental effects. In particular highly intermittent data with strong fluctuations may dominate less intermittent data having a weaker signal strength. If it is known that these differing statistics are the result of distinct physical processes, it is imperative that they be separated prior to analysis. Only through systematic studies of this nature can one make progress in perhaps solving the reverse problem in which one infers the likely physical mechanisms from the multiscaling / multiaffine statistics.

The sensitivity of multiscaling / multiaffine analysis to fluctuations of all magnitudes is a distinct advantage that these methods have over 1st order statistics or any other fixed order statistics. It is however a two-edged sword as instrumental artifacts, if ignored, may lead to strongly biased results. Quantization leads to noticeable changes in $K(q)$ for very small q and introduces an effective moment q_{min} below which moments are dominated by the quantization and possible introduction of zeroes. Apart from this, $K(q)$ and β are robust to this artifact.

Additive noise affects the $K(q)$ curve over a broader range of q than quantization, however again $K(q)$ and β are robust to small amounts of noise. The amount of noise that can be tolerated is dependent on the underlying process. Nevertheless, even small amounts of noise and quantization

behave as strong additive noises following a gradient transformation as one would perform to analyze a multiaffine field and estimate its $K(q)$ function.

The dependence of analysis results on instrumental artifacts is illustrated by the analysis of real data containing a spurious glitch. Given the sensitivity of multiscaling analysis to such fluctuations, this example demonstrates the importance of making sure that data is void of such artifacts and ensuring that extreme values are real.

A final example of instrumental dependence is illustrated by comparing radar and rain gauge time series collected at high time resolutions. The radar data seems, in general, to be more intermittent than the gauge data despite the fact that the two instruments are essentially measuring the same rain but in different ways. This illustrates the importance of considering the impact of differing measurement techniques before comparisons between instruments and general conclusions about the nature of rainfall can be made.

Appendix. Canonical cascades and the moment scaling function, $K(q)$

Some theoretical properties of canonical cascades are reviewed here for the purposes of explaining the biases observed between the parameters used to simulate cascades above and the ones retrieved following the multiscaling analysis of the constructed cascades. This appendix contains no new theoretical developments and is based upon results suggested in Mandelbrot (1974), and Kahane and Peyriere (1976) using notation similar to that used by the latter authors.

Consider a homogeneous distribution of a field in one-dimension (i.e., a time series; extensions to higher dimensions carry over in a simple way) having the value R_0 over the time interval T. On the first step the interval is divided into two halves and each of them is assigned a value $R_1=R_0W(1)$ and $R_2=R_0W(2)$, respectively. Note that for simplicity each interval here is split into two halves (i.e., branching number of $b = 2$); however, one could also divide each interval into thirds or any other fraction. The randomly chosen weights, $W(i)$, are independently and identically distributed (iid) random variables produced by a generator satisfying the condition that $<W> = 1$.

An N-step cascade of a time series may thus be represented by

$$R_N(i_1,\ldots i_N) = R_0W(i_1)W(i_1,i_2)\ldots W(i_1,\ldots,i_N) \quad \text{(A1)}$$

where the set of binary indices, $i_1, \ldots, i_N$ indicates 2^N possible realizations of the random field and R_0 is a constant. The field at a coarser resolution denoted by $n < N$ found by degrading the N-step cascade so that,

$$R_n(i_1,\ldots i_n) = R_0W(i_1)W(i_1,i_2)\ldots W(i_1,\ldots,i_n)Z_{N-n}(i_1,\ldots,i_n) \quad \text{(A2)}$$

where Z_{N-n} is called the high frequency component (Mandlebrot, 1974) or dressing factor (Schertzer and Lovejoy, 1987) equal to

$$Z_{N-n}(i_1,\ldots,i_n)= 2^{n-N}\sum_{i_{n+1},\ldots,i_N} W(i_1,\ldots,i_{n+1})W(i_1,\ldots,i_{n+2})\ldots W(i_1,\ldots,i_N)\,. \quad \text{(A3)}$$

Z_{N-n} is a random independent variable dependent only on N-n.

Raising both sides of (A2) to the q^{th} power and taking the average of both sides yields

$$<R_n^q>=(<W^q>)^n<Z_{N-n}^q>\,. \quad \text{(A4)}$$

For $(N - n) \to \infty$ $<Z_{N-n}^q>$ may diverge for some $q > q_{crit}$. This property is known as the divergence of moments (Mandelbrot, 1974). Taking the logarithm of both sides of (A4),

$$\log_2<R_n^q>=n\log_2<W^q>+\log_2<Z_{N-n}^q>\,, \quad \text{(A5)}$$

one gets the approximate scaling relation for $b = 2$. For the log-normal cascades used above, $<Z_{N-n}^q> \approx 1$ and thus $\log_2<R_n^q>\approx n\log_2<W^q>$ and since $n = T/t$ one approximately obtains (2) above with $K(q) = \log_2<Wq>$.

In the construction of log-normal cascades above with the parameter, σ, the retrieved parameter, σ_{est}, is consistently less than σ because, although $<Z_{N-n}^q> \approx 1$, $<Z_{N-n}^q>$ roughly increases with N - n for $q > 1$ and decreases with N - n for $q < 1$. Via simulations, $<Z_{N-n}^q>$ can be simply estimated and are found to increase (decrease) relatively quickly (e.g., from 1 to ~1.1 for $q > 1$) for low N - n ($(N - n) < 6$) and then roughly stabilizes only very slowly increasing (decreasing). This accounts for the decrease in bias with increase in cascade length. Similarly, since the bias decreases $|K(q)|$, it has the opposite effect on estimated values of β. Values slightly exceed the expected value for canonical cascades. It is also found, however, that $\beta + K(2)$ slightly exceeds unity on the average.

Acknowledgments. The authors would like to thank C. D. Stow for use of the electronic gauges, as well as Kim Dirks and Roger Nathan who helped collect the data. Much thanks to Rebecca Godfrey for the final edits. Discussions with Geoff Pegram and Joanne Purdy were much appreciated. Finally the authors thank John Nicol, Alain Vandal, Anthony Davis and two anonymous reviewers for their suggestions which led to an improved paper.

References

Atlas, D. (Ed.), *Radar in meteorology: Battan memorial and 40th anniversary radar meteorology conference*, American Meteorological Society, Boston, 1990.

Austin, K. N., *High resolution rainfall studies on Norfolk Island*, M.Sc. thesis, Univ. Auckland, NZ, 1994.

Benzi, R., Biferale, L., Crisanti, A., Paladin G., Vergassola, M., and Vulpiani, A., A random process for the construction of multiaffine field, *Physica D, 65*, 353-358, 1993.

Cahalan, R. F., Nestler, M., Ridgway, W., Wiscombe, W. J., and Bell, T., Marine stratocumulus spatial structure, in *Proceedings of the 4th international meeting on statistical climatology*, Rotorua, New Zealand, Sansom, J. (Ed.), New Zealand Meteorol. Service, Wellington, NZ, 1989, pp.28-32, 1989.

Davis, A., Marshak, A., Wiscombe, W., and Cahalan, R., Multifractal characterizations of nonstationarity and intermittency in geophysical fields: Observed, retrieved, or simulated, *J. Geophys. Res., 99(D4)*, 8055-8072, 1994.

Davis, A., Marshak, A., Wiscombe, W., and Cahalan, R., Scale invariance of liquid water distributions in marine stratocumulus. Part I: Spectral properties and stationarity issues, *J. Atmos. Sci., 53(11)*, 1538-1558, 1996.

Davis, A., Marshak, A., Wiscombe, W., and Cahalan, R., Multifractal characterizations of intermittency in nonstationary geophysical signals and fields. A model based perspective on ergodicity issues illustrated with cloud data, in *Current topics in nonstationary analysis*, Treviño, G., Hardin, J., Douglas, B., and Andreas, E. (Eds.), pp. 97-158, World Scientific, Singapore, 1996b.

Davis, A., Marshak, A., Gerber, H., and Wiscombe, W., Horizontal structure of marine boundary-layer clouds at 4 cm resolution: Scale break at 2-5 m, non-Poissonian behaviour at small scales, multifractal behavior at large scales, *J. Geophys. Res.*, (submitted), 1997.

Duncan, M. R., *The universal multifractal nature of radar echo fluctuations*, PhD Thesis, McGill University, Montreal, Canada, 1993.

Fabry, F., On the determination of scale ranges for precipitation fields, *J. Geophys. Res., 101(D8)*, 12819-12826, 1996.

Foufoula-Georgiou, E. and Krajewski, W., Recent advances in rainfall modeling, estimation and forecasting, U.S. Natl. Rep. Int. Union Geod. Geophys: 1991-1994, *Rev. Geophys.*, 1125-1137, 1995.

Georgakakos, K. P., Carsteanu, A. A., Sturdevant, P. L., and Cramer, J. A., Observation and analysis of midwestern rain rates, *J. Appl. Meteorol., 33*, 1433-1444, 1994.

Gupta, V. and Waymire, E., A statistical analysis of mesoscale rainfall as a random cascade, *J. Appl. Meteor., 32*, 251-267, 1993.

Hamburger, D., Biham, O., and Avnir, D., Apparent fractality emerging from models of random distributions, *Phys. Rev. E, 53(4)*, 3342-3358, 1996.

Harris, D., Menabde, M., Seed, A., and Austin, G. L., Multifractal characterization of rain fields with a strong orographic influence, *J. Geophys. Res., 101(D21)*, 26 405-26 414, 1996.

Hosking, G. J., Stow, C. D., Bradley S. G., and Gray, W. R., An improved high-resolution rainfall-intensity gauge, *J. Atmos. Ocean. Technol., 3*, 536-541, 1985.

Kahane, J. P. and Peyriere, J., Sur certaines martingales de Benoit Mandelbrot, *Adv. Math., 22*, 131-145, 1976.

Lavallée, D., Lovejoy, S., Schertzer, D., and Ladoy, P., Nonlinear variability of landscape topography: Multifractal analysis and simulation, in *Fractals in geography*, Lam, N. and De Cola, L. (Eds.), pp.158-192, Prentice Hall, 1993.

Lovejoy, S. and Schertzer, D., Multifractal analysis techniques and the rain and cloud fields from 10^{-3} to 10^{6}, in *Non-linear variability in geophysics. Scaling and fractals*, Schertzer, D. and Lovejoy, S. (Eds.), pp. 111-144, Kluwer, Netherlands, 1991.

Lovejoy, S. and Schertzer, D., Multifractals and rain, in *New uncertainty concepts in hydrology and water resources*, Kundzewicz, A. W. (Ed.), pp. 61-103, Cambridge Univ. Press, New York, 1995.

Marshak, A., Davis, A., Cahalan, R., and Wiscombe, W., Bounded cascade models as nonstationary multifractals, *Phys. Rev. E, 49(1)*, 55-69, 1994.

Mandelbrot, B., Intermittent turbulence in self-similar cascades: Divergence of high moments and dimension of the carrier, *J. Fluid Mech., 62(2)*, 331-358, 1974.

Mandelbrot, B., *The fractal geometry of nature*, W.H. Freeman and Co., New York, 1983.

Menabde, M., Harris, D., Seed, A. W., Austin, G. L., and Stow, C. D., Multiscaling properties of rainfall and bounded random cascades, *Water. Resour. Res.,33(12)*, 2823-2830, 1997.

Perica, S. and Foufoula-Georgiou, E., Model for multiscale dissaggregation of spatial rainfall based on coupling meteorological and scaling descriptions, *J. Geophys. Res., 101(D21)*, 26 347-26 361, 1996.

Press, W. H., Teukolsky, S. A., Vetterling, W. T., and Flannery, B. P., *Numerical recipes in C: The art of scientific computing, 2nd ed.*, Cambridge University Press, 1992.

Purdy, J. C., *Rainfall enhancement processes. A case study*, M.Sc. thesis, Univ. Auckland, NZ, 1997.

Rodda, J. C., The precipitation measurement paradox: The instrument accuracy problem, *WMO Report No. 316*, Geneva, 1971.

Saito, Y., Log-gamma distribution model of intermittency in turbulence, *J. Phys. Soc. Japan, 61(2)*, 403-406, 1992.

Schertzer, D. and Lovejoy, S., Physical modeling and analysis of rain and clouds by anisotropic scaling multiplicative processes, *J. Geophys. Res, 92(D8)*, 9693-9714, 1987.

Schertzer, D. and Lovejoy, S., Hard and soft multifractal processes, *Physica A, 185*, 187-194, 1992.

Seed, A. W., Nicol, J., Austin, G. L., Stow, C. D., and Bradley, S. G., The impact of radar and raingauge sampling errors when calibrating a weather radar, *Meteorol. Appl., 3*, 43-52, 1996.

Smith, J. A. and Krajewski, W. F., A modeling study of rainfall rate-reflectivity relationships, *Water Resour. Res., 29(8)*, 2505-2514, 1993.

Stow, C. D., Bradley, S. G., Farrington, K. E., Dirks, K. N., and Gray, W. R., A rain gauge for the measurement of fine scale temporal variability, *J. Atmos. Ocean. Tech.*, (in press), 1997.

Taylor, J. R., *An introduction to error analysis. The study of uncertainties in physical measurements*, Oxford University Press, 1982.

Vainshtein, S. I., Sreenivasan, K. R., Pierrehumbert, R. T., Kashyap, V., and Juneja, A., Scaling exponents for turbulence and other random processes and their relationships with multifractal structure, *Phys. Rev. E, 50(3)*, 1823-1835, 1994.

Yaglom, A. M., *Correlation theory of stationary and related random functions. Volume I: Basic results*, Springer-Verlag, New York, 1987.